PASSIVATED IMPLANTED PLANAR SILICON (PIPS) DETECTORS FOR MEASUREMENT OF RADIOXENON

A Dissertation
Presented to
The Academic Faculty

by

Peter Sobel

In Partial Fulfillment
of the Requirements for the Degree
Masters of Science in
Nuclear and Radiological Engineering

Georgia Institute of Technology
December 2020

PASSIVATED IMPLANTED PLANAR SILICON (PIPS) DETECTORS FOR MEASUREMENT OF RADIOXENON

Approved by:

Dr. Steven Biegalski, Advisor
School of Mechanical Engineering
Georgia Institute of Technology

Dr. Anna Erickson
School of Mechanical Engineering
Georgia Institute of Technology

Dr. Michael Foxe
Staff Scientist
Pacific Northwest National Lab

Date Approved: December 1, 2020

In dedication to Abby, Marshmallow and Opie.

ACKNOWLEDGEMENTS

Thank you to Dr. Biegalski, Dr. Erickson, and Dr. Foxe for being on my committee and supporting me in my work. Special thanks to all my graduate student friends for your academic and moral support during my time at Georgia Tech.

TABLE OF CONTENTS

LIST OF TABLES

LIST OF FIGURES

LIST OF SYMBOLS AND ABBREVIATIONS

2D	Two-Dimensional
BEGe	Broad Energy Germanium
CTBT	Comprehensive Nuclear-Test-Ban Treaty
HPGe	High Purity Germanium
IMS	International Monitoring System
LN_2	Liquid Nitrogen
MCA	Multichannel Analyzer
NaI(Tl)	Sodium Iodide
PHA	Pulse Height Analysis
PIPS	Passivated Implanted Planar Silicon
PMT	Photomultiplier Tube
PSD	Pulse Shape Discrimination
^{131m}Xe	Xenon 131m
^{133}Xe	Xenon 133
^{133m}Xe	Xenon 133m
^{135}Xe	Xenon 135

SUMMARY

The International Monitoring System arm of the Comprehensive Nuclear-Test-Ban Treaty Organization in part utilizes sampling of atmospheric radioxenon to scan the world for nuclear testing events. Radioxenon has a natural abundance in the atmosphere but is also a commonly released byproduct of fission reactions involving heavier atoms. Due to its inert nature and short half-life, the gas makes an excellent indicator of recent nuclear activity. With that given, differentiating the signatures released from nuclear power plants, nuclear testing, and medical isotope production facilities requires a fast, high resolution detection system.

Current designs utilized in the field involve plastic scintillator cells run in coincidence with NaI(Tl) or HPGe detectors. The use of plastic scintillators as electron detectors exhibit some issues in comparison to other materials. The energy resolution tends to be lower and the diffusion of gas into the plastic creates long-term signal degradation. Silicon detectors are analyzed as an alternative to plastic scintillators for beta detection based on their higher energy resolution and lowered memory effect.

A radioxenon detection setup was created with the intent of measuring radioxenon samples using coincidence counting between silicon and NaI(Tl) detectors as well as silicon and HPGe. The absolute efficiency of both setups is calculated and compared.

CHAPTER 1. INTRODUCTION

This chapter contains discussion on the state of the nuclear forensics field, the objectives of the work, and a description of analysis of radioxenon data.

1.1 Motivation

The final draft of the Comprehensive Nuclear Test Ban Treaty (CTBT) was first proposed in 1996 and set forth guidelines for putting a halt to construction of further nuclear weapons and dismantling old ones. As part of the creation of this treaty, countries included have begun operation of an International Monitoring System (IMS) program involving use of seismic, hydroacoustic and nuclear signature detection systems. The detection of nuclear signatures is done through both radioactive particulates and noble gas measurements. Detection of radioxenon is currently performed in the field utilizing mainly plastic scintillators and with photon detectors performing coincidence measurements. Coincidence measurements between electrons and photons allow for effective removal of background signatures in air samples and to properly discriminate between the four major radioxenon isotopes. Plastic scintillators have shortcomings as electron detectors due to lower energy resolution and memory effect problems. The goal of this work is to characterize improvements in the use of silicon as a beta detector instead.

1.2 Objectives

The purpose of this thesis is to perform measurements of radioxenon using passivated implanted planar silicon (PIPS) detectors and perform a comparison of the data obtained using different photon detectors. To accomplish this goal, first a radioxenon detection

laboratory would have to be created. The laboratory requires multiple features: a gas containment system, a detection system, and an electronics system for data collection. Next two types of measurements need to be performed:

- Counting measurement of radioxenon using a passivated implanted planar silicon semiconductor with a sodium iodide (NaI(Tl)) scintillator.
- Counting measurement of radioxenon using a passivated implanted planar silicon semiconductor with a high purity germanium (HPGe) semiconductor.

The collected data can be analyzed to examine the characteristics of each setup and a comparison of NaI(Tl) and HPGe beta-gamma coincidence spectra can be performed.

1.3 Thesis Outline

The structure of the thesis will be laid out in the following manner. Chapter 2 will include background information on radioxenon gas, the different sources of radioxenon in the atmosphere, and on historical methods of radioxenon detection and the technologies involved. All information shown is presented from publicly available sources. Chapter 3 will go over the experimental setup created, including the gas manifold, detectors, and the electronics used. Chapter 4 will provide the methodology used to collect data, including operation of the CAEN software used. Chapter 5 will present some accumulated spectra and present the comparison calculations of the two setups absolute efficiency. Finally, Chapter 6 will contain the conclusion and future work sections.

CHAPTER 2. BACKGROUND

This chapter contains an explanation of the characteristics of radioxenon that make it an attractive detection target. Sources of radioxenon in the atmosphere are discussed. Finally, past and current designs used for radioxenon detection are mentioned.

2.1 Radioxenon

Nuclear weapons pose a constant risk to national security and have been the source of looming threat over the 21st century. The acknowledgement of the issue with creation and testing of nuclear weapons has led to the inception of the CTBT, a treaty banning all nuclear testing and creating the need for a global detection arrangement. The important job of detecting atmospheric nuclear signatures has fallen onto a large network of stations as part of the IMS. While the system is comprised of detection systems using seismic, hydroacoustic and other data, only radioactive xenon measurements allow for monitoring of the air as a method to determine if nuclear testing has been performed covertly underground [1].

Xenon, as a noble gas, is an ideal carrier of information for nuclear forensics purposes. As an inert gas, it does not react chemically with shielding used to hide nuclear testing. It is capable of passing through the ground after a test has occurred, with the primary losses as it passes through earth being through adsorption on sediment.

There are four major radioxenon isotopes that are used in the identification of atmospheric nuclear signatures. Each isotope is found in the atmosphere due nearly entirely to anthropogenic sources. The four isotopes are ^{131m}Xe, ^{133}Xe, ^{133m}Xe, and ^{135}Xe. The most commonly observed form of atmospheric radioxenon is ^{133}Xe. As its half-life is 5.243 days

it exists for long enough to be measurable but not long enough to influence background measurements in the long term.

When distinguishing the potential sources of radioxenon in the atmosphere, a common method is through analyses of the ratios of the metastable xenon isotopes and the other two radioactive isotopes. Each isotope has a different half-life and expected release based on the exact source of the radiation. Additionally, the decay modes of each isotope vary by process and energy. Table 2.1 lists the four radioxenon isotopes and describes their various decay energies.

Table 2.1 Primary Radioxenon Isotopes Energies

Nuclide	^{131m}Xe	^{133m}Xe	^{133}Xe	^{135}Xe
Gamma energy (keV)	163.9	233.2	81.0	249.8
X-ray energy (keV)	29.5-34.6	29.5-34.6	30.6-36.0	30.6-36.0
Beta endpoint energy (keV)			346	905
Conversion electron energy (keV)	129	199	45	214

2.2 Radioxenon Sources

Radioactive xenon in the air can come from a variety of sources, leading to the need for accurate measurements of the four isotopes in small concentrations. Expected

concentrations of the isotopes released depends on the initial source. The four major sources are discussed in the following sections.

2.2.1 Naturally Occurring Radioxenon

The Earth's atmosphere contains approximately 0.087 ppm of stable xenon. For the most part, radioxenon contained within air samples is manmade. Primary natural sources come from spontaneous fission of uranium in nature and air activations of xenon from cosmic rays. In total approximately 24% of the yields from uranium or plutonium fissions are noble gases, with xenon isotopes being the majority [2].

2.2.2 Nuclear Power Plants

Radioxenon is an important factor in the operation of nuclear power plants, as ^{135}Xe is commonly created as a daughter of ^{135}I. ^{135}Xe in a nuclear power plant acts as a neutron absorber and is otherwise known as a significant source of poison to a nuclear reactor.

Radioxenon created in most nuclear power plants is generated within the fuel rods in the reactor and is retained there. Thus, the release of xenon from power plants is not nearly as huge a source as radiopharmaceutical companies despite the similar processes [3]. Estimates for total release of radioxenon in a generic year were estimated to be 1.3 PBq from nuclear power plants alone in 2009 [4].

An example of potential xenon releases from a power plant accident can be identified from the Fukushima Daiichi nuclear reactor incident in 2011. US monitoring stations measured levels of ^{133}Xe in the air of up to 17 Bq m^{-3}, much above the minimum detectable concentrations needed by IMS standards [5].

2.2.3 Radiopharmaceutical Industry

^{133}Xe is a commonly produced isotope for the purposes of medical imaging. It is typically used for measuring the parameters of lungs and imaging. The use of ^{133}Xe is on the decline however with the increased availability of ^{99m}Tc.

It was found that large spikes in radioxenon background were coming from a few radiopharmaceutical manufacturers during production of medical radioisotopes. Mean activity of ^{133}Xe in the air for various stations around the world show the effect of nearby nuclear power plants and radiopharmaceutical plants. The International Noble Gas Experiment radioxenon station in Ottawa which is located 150 km from where Chalk River was located would measure spikes of 1-10 Bq m^{-3}. Production of ^{131m}I gives rise to its daughter nuclide ^{131m}Xe which often escapes into the atmosphere during reprocessing. Most noble gas releases from nuclear reactors occurs from cracking in fuel rod cladding while radiopharmaceutical releases occur during chemical separation.

A radioisotope production facility that irradiates for two days and releases radioxenon within seven will closely resemble the signal of a nuclear explosion. Radioxenon stations with high time resolution were able to lower overall measurement times to 12 to 24 hours and identify all four radioxenon isotopes. Literature showed that the combined release of all nuclear power plants worldwide was 0.74×10^{15} Bq of ^{133}Xe while the four largest radiopharmaceutical companies alone released 11×10^{15} Bq of ^{133}Xe per year [6].

Implementation of strict xenon release goals for radiopharmaceutical companies are potentially not practical. Mixing in natural xenon as tracer can shift the radioxenon

isotopic ratios away to the left from the region where nuclear detonations reside. Barium and Cesium can significantly alter the Xenon ratios but are impractical to manufacture in quantities large enough for irradiation. Stable tracers such as Sulfur Hexafluoride and ^{3}He have been examined but SF_6 is a greenhouse gas and ^{3}He is no longer produced and quite expensive. Metal particulates have also been examined, however these tracer would need to be detected through means such as neutron activation analysis or X-ray fluorescence, which the IMS network currently does not include [7].

2.2.4 Nuclear Testing

After the claimed nuclear test by the Democratic People's Republic of Korea in 2006, a detection setup in the Republic of South Korea sampled atmospheric air in the days following. In the case studied, sampling was performed in the 72-132 hours after the explosion, with measurements occurring in the 6-13 days after. A maximum concentration of ^{133}Xe was found to be 7 mBq. A 1 kt device would release about 10^{16} Bq, which meant this measurement was compatible with a 0.7% release of radioxenon from the test site. Measurable quantities of ^{133}Xe and ^{133m}Xe were observed with concentrations potentially characteristic of a nuclear test [8].

2.3 Radioxenon Detection

Under the IMS regime there have been four main systems that are deployed globally to measure radioxenon gas captured from the air. They are the Automated Radioxenon Sampler Analyzer (ARSA), Automatic Radioanalyzer for Isotopic Xenon (ARIX), Swedish Automatic Unit for Noble Gas Acquisition (SAUNA), and the Syste`me de

Pre´le`vement Automatique en Ligne avec l'Analyse du Xe´non (SPALAX). Table 2.2 lists the four major systems and their detection setup.

Table 2.2 Main Features of the Four Systems [9]

System	Activity Measurement	Sampling Cycle (h)	Eff. Air Volume Sampled (m^3)
SPALAX	High purity germanium detector	24	29.5
ARSA	Beta-gamma coincidence, gamma energy and beta energy	8	19.9
ARIX	Beta-gamma coincidence, gamma energy	12	8.2
SAUNA	Beta-gamma coincidence, gamma energy and beta energy	12	5.9

2.3.1 ARSA

The ARSA system was first prototyped in 2000 by Pacific Northwest National Laboratory to fulfil CTBT minimum detectable requirements for ^{133}Xe of less than 1 mBq m^{-3} of air for a 24-hour sampling period. The detection system was compromised of four plastic beta cells surrounded by two NaI(Tl) scintillator crystals. The full apparatus compromised a nearly 4π counting system. The plastic beta cells were made of 1.2mm thick plastic formed into 5 cm long hollow tubes. Each cell ended with a photomultiplier tube (PMT) allowing for light collection to be converted into voltage pulses. The NaI(Tl) crystal were manufactured as 5" by 8" planes with three PMTS adjoined to each face. Each cell ended with a photomultiplier tube (PMT) allowing for light collection to be converted into voltage pulses. Figure 2.1 shows the design of ARSA at the time.

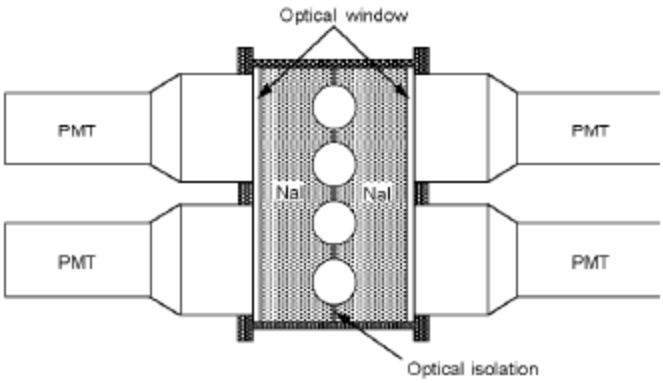

Figure 2.1 ARSA Design [10]

The counting system utilized a beta-gamma coincidence setup to individually detect the four xenon isotopes. The detection cell was found to have an approximately 5% memory effect from previous xenon samples. The highest MDC for ^{133}Xe was found to be 0.39 mBq m^{-3} [10].

In 2007 a redesign was performed on the ARSA model to simplify the system while retaining its strong MDC characteristics. The new setup utilized a single well detector for photons and a single PMT gas cell for the charged particles. Three different photon sensitive scintillators were tested, NaI(Tl), CsI(Na), and CsI(Tl). After each were tested a switch to CsI(Na) was made as it had the highest density, and best temperature independence. The beta cell was also converted to require only one PMT negating the need for gain matching [11].

2.3.2 ARIX

ARIX was developed at the NPO Khlopin Radium Institute. The ARIX system used a NaI(Tl) scintillator much as ARSA did for photons but switched out the plastic scintillator

for an organic polystyrene scintillator applied to the walls of the measurement chamber. The measurement chamber was an aluminium barrel placed within the well of the NaI(Tl) crystal to maximize efficiency in detecting γ-rays. PMTs were placed on opposite ends of the measurement chamber to collect the light from the beta cell and NaI(Tl) individually. Figure 2.2 depicts a diagram of the detection setup.

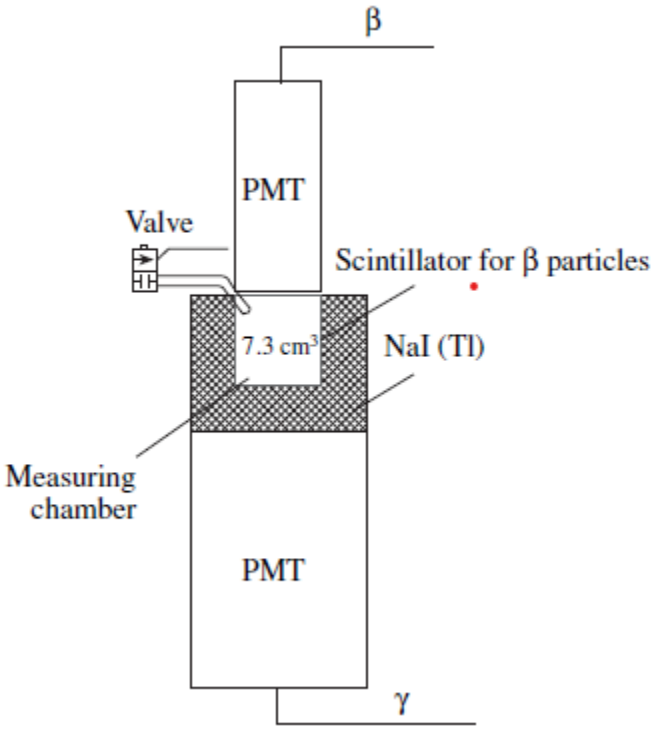

Figure 2.2 ARIX Design [12]

Much like ARSA, the ARIX design also operated using the beta-gamma coincidence principle. Results from the detectors were an MDA of 6.2 (^{131m}Xe), 6.6 (^{133m}Xe), 4.8 (^{133}Xe), and 7.7 (^{135}Xe) mBq respectively. These convert to an MDC of approximately 0.5 mBq m^{-3} [12].

2.3.3 SAUNA

SAUNA was developed by the Swedish Defence Research Agency as a detection module and collected and shared its data as part of the International Noble Gas Experiment. Gas collection from air occurred similarly to the other radioxenon analysers, using activated charcoal to have xenon adsorb onto the surface. A push in this case was to remove the need for cooling of the activated charcoal system (removing power consumption and simplifying the system greatly). Air processed in the system was cleaned in molecular sieves to remove water and CO_2. Adsorption of charcoal for xenon was found to be 1000 cm^3/g. A gas chromatograph was used to quantify the amount of extracted xenon.

The setup consisted of two coincidence detectors placed inside lead-copper radiation shields. Beta detectors similar to those in ARSA were manufactured from BC404 plastic scintillator material shaped into cylinders. Thickness of the cylinders were made to be 1 mm to fully stop 350 keV electrons. Two PMTs were affixed to either end for light collection. In a similar setup to ARSA, the use of NaI(Tl) scintillators with a PMT for photon detection. Figure 2.3 demonstrates the setup, with the beta detectors inserted through the NaI(Tl) cylinder.

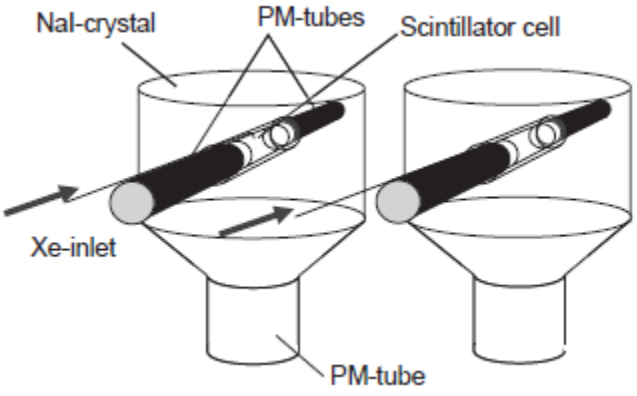

Figure 2.3 SAUNA Design [13]

Memory effect of this setup was found to be on the order of 3-4% of the sample activity. Average MDC's for all four radioxenon isotopes were well below the 1 mBq m^{-3} requirement and went down to 0.1-0.2 mBq m^{-3}. Attempts to reduce the memory effect while maintaining efficiency and energy resolution were later made using a modified Al_2O_3 coated plastic scintillator cell. Effects on resolution were found to be comparable to uncoated detectors while the reduction in memory effect was about a factor of 1000. [14]

2.3.4 SPALAX

Prototyped by the French Atomic Energy Commission (CEA) in 2000, this detection setup operated on a principle of solely utilizing γ spectrometry to analyze radioxenon samples. A fully automated system, gas collection operated on a coupled gas permeator and charcoal collector for air cleaning and xenon adsorption. The detector itself was a HPGe cooled by an electric cryostat. Pure gamma spectrometry was selected over beta-gamma spectrometry as it allowed for direct measurement of the four radioxenon isotopes. In a 24-hour sampling period, MDC of 133Xe was 0.15 mBq m^{-3} [15].

An improved version of the SPALAX system was developed in 2013 in collaboration with the Canberra Semiconductors company to rectify issues with the pure gamma measurements. The decision was made to switch to a beta-gamma coincidence system as the other three major efforts had produced. A PIPSbox silicon semiconductor detector was used for measurement of betas and conversion electrons. The two silicon detectors measured 500 µm thick with a 1200 mm^2 surface area. The photon measurements were made via a BEGe. The model BEGe 5030 is 30 mm thick with a 50 cm^2 area crystal.

Shielding on the experiment was provided by a 5 cm layer of low activity lead [16]. Figure 2.4 displays the detectors used.

Figure 2.4 SPALAX Experiment with PIPSbox and HPGe Detector [16]

CHAPTER 3. EQUIPMENT

The following chapter includes sections covering the description of the physical experimental equipment, including the detectors, gas manifold, high voltage, and data acquisition electronics. Additionally, the software interfacing with the electronics will be mentioned.

3.1 Detectors

The general principle for the operation of a beta-gamma coincidence detection system requires two detectors. A detector for conversion electrons and beta particles is run in a coincidence timing window with a detector for photons (X-rays and Gamma-rays). This work utilized two different photon detectors to compare results of beta-gamma coincidence.

3.1.1 Passivated Implanted Planar Silicon (PIPS)

For beta detection a passively implanted planar silicon semiconductor was selected. The basis for selection was to provide avenues of comparison to the more commonly used plastic scintillator cells previously discussed which have a much lower energy resolution.

Semiconductor detectors are fabricated as a PN junction with a depletion zone. The depletion zone is created by biasing a region of opposing polarities creating a zone in which any incident radiation energy deposited will free electrons from the valence band. The freed electrons produce a current in the semiconductor material which is carried then to the

preamplifier for shaping and amplification. Information about the energy deposited in the detector is analysed based on the total amount of charge collected by the preamplifier.

The laboratory acquired a Mirion Technologies PIPSbox for this purpose. The design of this detector was compromised of two silicon detectors encapsulating an empty cell with a port which was utilized as the gas testing cell. Specifications for both silicon were given as 1200 mm^2 active surface area with a silicon thickness of 500 µm, significantly thick enough to allow for full deposition of electrons up to 350 keV. The detectors and gas cell were confined by an aluminium housing with carbon windows to block sources of external radiation (mainly photons). These detectors required no cooling for operation and boasted a minimal temperature instability (<100 ppm/ °C) in the realm of room temperature (0 to 50 °C). The PIPSbox could be operated in any orientation but did not stand on its own in a vertical orientation. To facilitate using the detector upright with both windows facing an NaI(Tl) detector a plastic stand was designed and printed. Figure 3.1 is an image of the PIPSbox detector in its vertical orientation with the printed stand.

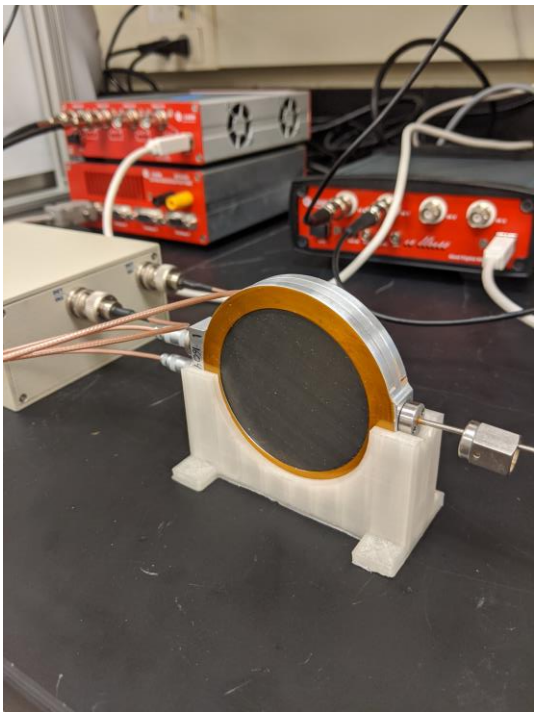

Figure 3.1 PIPSbox in Stand

3.1.2 Sodium Iodide

NaI(Tl) detectors are inorganic scintillators which produce light when absorbing energy from radiation. The light emitted is wave shifted using dopant materials in the crystal, allowing produced light to travel to the PMT without reabsorption. The PMT contains a photocathode which absorbs the photon and releases an electron, which is multiplied and collected. The amount of light produced by the NaI(Tl) crystal thus corresponds to a certain number of electrons, the information the system needs to deduce the energy of the radiation.

Two different NaI(Tl) scintillators were used at points for experimentation. Two Canberra model 802 were brought in with crystals measuring 2” by 2”. These detectors came with a built in PMT for light collection and were slightly used leading to potentially some discrepancies with data collected from them.

Bought new for the experiment were also two Scionix model 51B51/2M-E1. These models were selected as they came with built-in voltage dividers and were well suited for the energy range (rated to go as low as 20 keV). Dimensions of the crystal were 220 mm length by 59 mm diameter. The two NaI(Tl) detectors are depicted in Figure 3.2.

Figure 3.2 Canberra NaI(Tl) (left) and SCIONIX NaI(Tl) (right)

3.1.3 High Purity Germanium

HPGe detectors operate in a similar fashion as the silicon detectors, both being a semiconductor type detector with a depletion zone in which radiation can deposit its energy and be converted to a current. Germanium however has a much lower bandgap energy, and thus suffers from easy thermal excitations of electrons at room temperature. In order to operate a germanium detector, the system must be cooled to a low enough temperature that thermal excitations no longer dominate the interactions. This cooling is typically provided by a source of liquid nitrogen, which can bring the detector down to 77K.

The germanium detector utilized was a Canberra BE3825 which is specifically a BEGe. Portable HPGe's available were unable to detect X-rays and low energy γ-rays in the energy region of interest and thus the need for a broad energy photon detector necessitated using a BEGe instead. Detectors dimension were 38 cm^2 with a thickness of 25 mm and a given relative efficiency of 26%. Energy resolution was specified as 0.45 at 5.9 keV and 0.72 at 122 keV.

The detector itself was contained within a large cylindrical lead shield with a rotatable cap. As it was a germanium detector, constant cooling was required and provided by a liquid nitrogen cryostat filled regularly. The detector was fixed within its lead shielding at a certain height. The HPGe in its shielding is shown in Figure 3.3

Figure 3.3 Germanium Detector within Shielding

3.2 Gas Manifold and Control

The gas manifold was designed to allow a straightforward method of controlling the flow of vacuum pumping. Controls also allowed for easy purging of radioxenon samples by inert “cleaning” gases such as nitrogen to help remove old samples of gas left in the pipes. Figure 3.4 shows the manifold design.

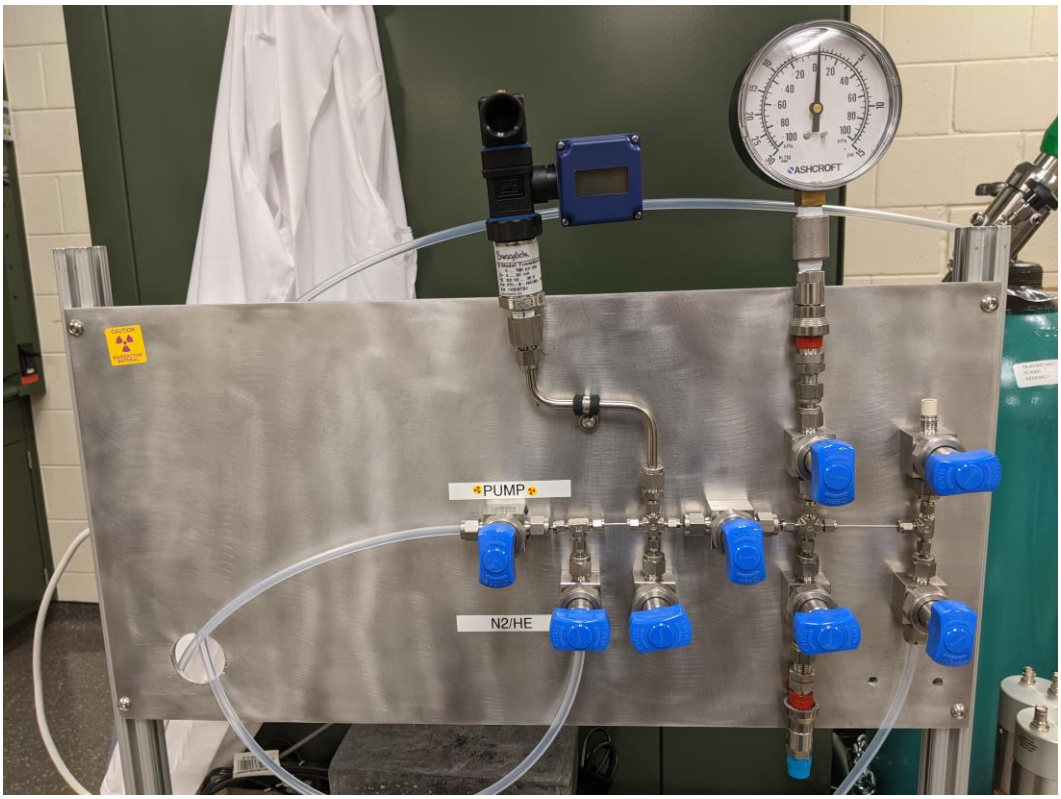

Figure 3.4 Gas Manifold

The valves, fittings, and pressure regulators were all Swagelok. Vacuum pumping was provided by an Agilent Technologies model X3810-64000. A simple pressure gauge was included on the testing side of the apparatus to monitor loss of vacuum during testing. A line to a low-pressure regulator on a nitrogen bottle was included to allow for sweeping out old test gas and air between experimental runs.

^{133}Xe samples were obtained from the Lantheus Medical Imaging company. Xenon gas samples were received in rubber capped sample vials. Injection of the samples into the gas manifold was accomplished using a Hamilton gastight syringe. A rubber septum installed on one port gave a leak tight seal which could be penetrated for gas injection. The syringe and sample vial are shown in Figure 3.5.

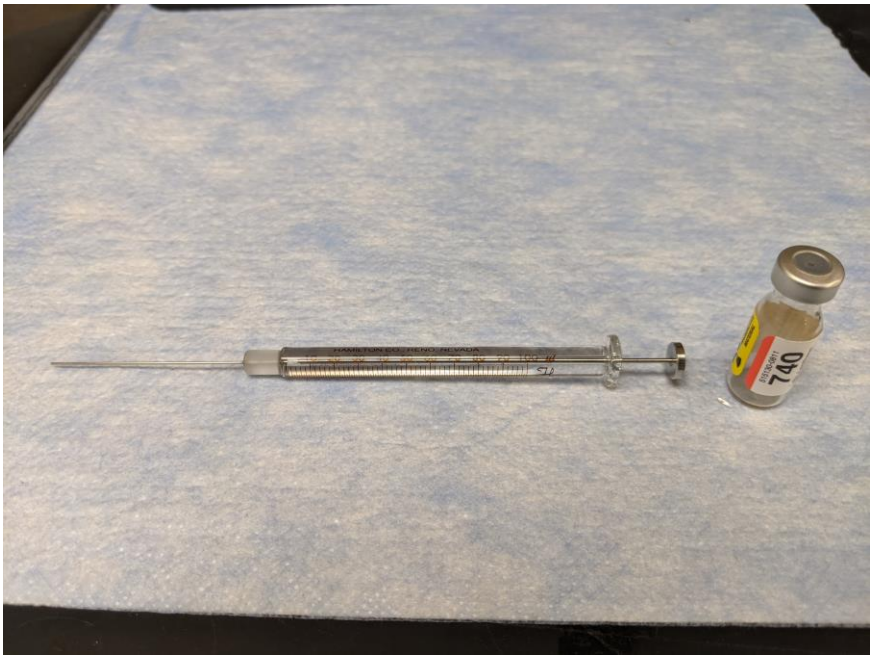

Figure 3.5 Hamilton Syringe and ^{133}Xe Sample Vial

3.3 Electronics

Electronics for the detectors were provided by three desktop CAEN modules. Power to the electronics was run through a Tripplite isolation transformer to sanitize any signal noise that could be picked up from the buildings electricity. A CAEN DT5423 with four outputs was used for low voltage power distribution of preamplifiers. This model was effectively capable of supplying power to up to four preamplifiers or PMTs, enough to do coincidence with both silicon detectors.

A Mirion Technologies preamplifier designed for use with the PIPSbox was used to bias the silicon detectors and collect the charge information. The preamplifier boasted a specialization in situations where low noise is required. The sensitivity was given as 400 mV/MeV and had an output range of ±3.5 volts on a 50 Ω termination. The device featured high voltage inputs, detector signal inputs, and energy signal outputs for both detectors.

The high voltage was provided by a CAEN DT5533EM mixed power supply. The characteristics needed for the supply was availability of negative and positive polarity high bias voltage for the silicon and NaI(Tl) detectors, respectively. Additionally, this power supply was chosen as it was necessary to be able to bias detectors up to 1000 volts while having an input current control granularity on the order of 5 nA.

A CAEN DT5781 Quad Digital Multi Channel Analyzer (MCA) functioned as the digital pulse processor and data acquisition system. The system came with four independent 16k channel digital multi-channel analyzers for up to 4 detectors. The duty of the MCA was to take in signals coming in from the preamplifiers and PMT's of detectors and generating a trigger logic on pulses of appropriate height. A lower energy threshold was set to keep accepted pulses above the noise and pulse pile up conditions set by the user are used to remove spurious pulses. Energy pulses accepted by the system are passed through a digital Jordanov trapezoidal filter whose trapezoidal flat top corresponds to the original energy of the incident radiation. The system than binned the count based on its energy into its corresponding channel. Built in logic to perform coincidence and anti-coincidence measurements between separate channels were also a feature of the MCA. A picture of the desktop electronics modules is included as Figure 3.6

Figure 3.6 Electronics Setup for PIPSbox

3.4 Software

All software was installed and run on a Dell laptop computer utilizing the Windows 10 operating system.

Software controls were provided by CAEN to interface with their own electronics. Interfacing between the electronics and software controller was done through a USB connection. CAEN GECO2020 software was used to control the bias voltage supplied to both silicon detectors and all NaI(Tl) detectors. The software allowed for independent control of bias voltage to all detectors and gave monitoring status of applied voltage and current draw.

CAEN Multi-Parameter Spectroscopy Software (COMPASS) was used to interface with the MCA board and control the parameters used to analyze the incoming detector

signals. While the software had functionality for digital pulse processing of pulse shape discrimination (PSD) and pulse height analysis (PHA) only the PHA features are utilized. The software allows for two modes of data collection, a wave mode and a list mode. In wave mode, the incoming signal was plotted as a function of time and captured the moment that a trigger occurs. In list mode all events were recorded as time stamped data, with the capability of saving both energy and channel binned data. The data files could be saved in a few formats, notably as CSV files and ROOT files. Analysis of the collected data was done entirely in MATLAB.

CHAPTER 4. METHODOLOGY

The following chapter contains a complete description of the operation of the radioxenon laboratory as operated for this thesis. Discussion will first focus on the setup of the detectors and shielding, followed by the gas manifold and gas controls, and finally the use of the CAEN electronics and accompanying software.

4.1 Detector Setup

The detector system geometry impacted the quality of the measurements obtained and needed to be considered fully to maximise the coverage of the system. Detectors were kept close together to increase geometric efficiency of interactions with released radiation and to minimize the amount of shielding that needed to be used.

4.1.1 PIPSbox with NaI(Tl)

Four total detectors were utilized in the silicon-NaI(Tl) detector setup, to enable two different coincidence measurements. As the silicon detectors were both in parallel with opposite facing windows, the NaI(Tl) detectors were placed on opposite sides of the PIPSbox. The setup was placed directly below the gas manifold to minimize the tube connection to the measurement cell in the PIPSbox. Additionally, aluminium foil was wrapped around the PIPSbox to shield from any outside sources of photons. Electronics were kept on the workspace alongside them but left out of the shielding. Figure 4.1 shows the geometry of the coupled detectors.

Figure 4.1 Silicon and NaI(Tl) Detectors Aligned for Coincidence

Shielding for the detectors was comprised of 1-inch thick lead bricks. The bricks were stacked to create as little gap as possible for light to travel through while still leaving space for the cables and the gas line. Figure 4.2 depicts the completed shielding setup.

Figure 4.2 Lead Shielding Around the Detectors

4.1.2 PIPsbox with HPGe

The detector setup for measurements with the HPGe were simplified by having prebuilt copper-lined lead shielding already encasing the germanium detector. The experiment still had its own source of complications in the need to run the gas line from the manifold deep into the HPGe lead containment. The manifold was moved next to the HPGe stand and a long stainless-steel tube was run into the lead housing to the measurement cell. The PIPSbox itself was placed on top of a 3D printed plastic cover for

the HPGe to avoid damaging either detector's carbon window. Figure 4.3 depicts the PIPSbox resting on the cover protecting the HPGe window.

Figure 4.3 PIPSbox and HPGe Inside Shielding

The gas line and electronics cables were fed through a slit in the shielding out to the preamplifier on the other side. Figure 4.4 is an image of the gas manifold, electronics, and detector shielding. The clear tube shown running from the manifold to the shielding was the Xenon-133 gas transfer line.

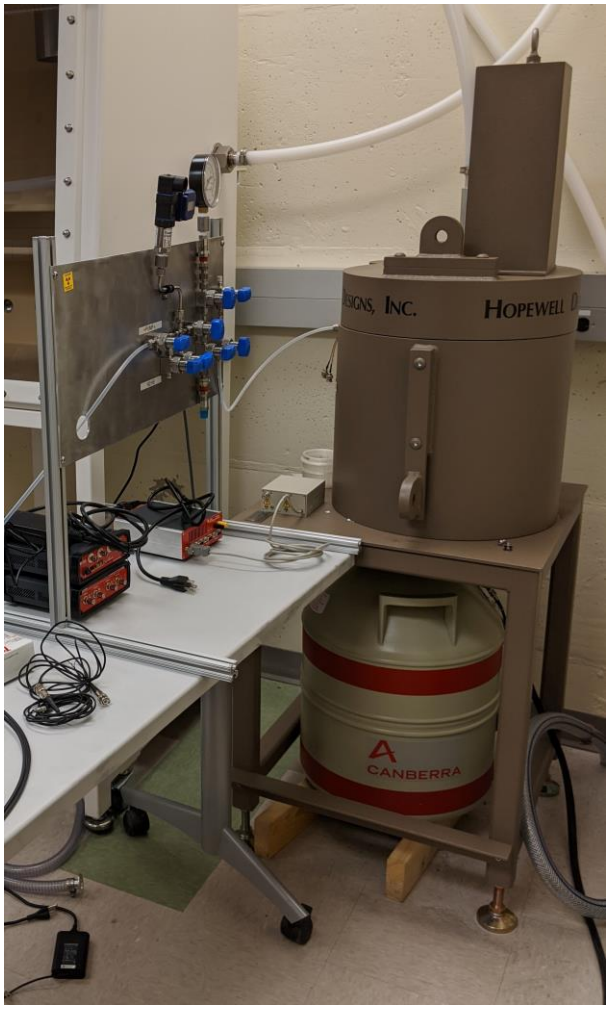

Figure 4.4 Configuration of Gas Manifold and HPGe Shielding

Cooling of the HPGe detector was done through filling of the cryostat at the base of the shielding with liquid nitrogen (LN_2). LN_2 arrived in large dewars with ports for dispensing liquid which could be connected to the fill port on the collar of the cryostat just under the HPGe stand. The procedure for liquid nitrogen filling was as follows.

1. Take the fill line and make the connection on the liquid port on the dewar. Teflon tape can be used to thread the connection on easier.

2. Connect the other end of the fill line to the fill port on the cryostat collar. Either port can be used for filling. The line should be held onto the fill port tube using a pipe clamp.
3. With both connections on tight, turn the valve slightly open to begin dispensing liquid. Nitrogen should be dispensed at a slow rate at first while the transfer line frosts up. Smoke will pour out of the exit port of the cryostat at this time.
4. After the line frosts up and the puffs of smoke coming from the cryostat become a more constant stream, the valve on the dewar can be opened further to increase flow rate.
5. The dewar takes a while to fill up and may go through some transitions along the way. As the metal cools it will contract and may make loud pinging noises. The puff of smoke exiting the outlet port will grow and shrink. Even at a fully opened valve the initial cooling of the detector can take some time. Be patient.
6. Once the dewar is full the stream of smoke exiting the outlet port converts to a stream of liquid nitrogen. The liquid stream is allowed to flow for a minute or two to top off the cryostat completely and finally the valve on the dewar is shut closed again.
7. After the cryostat is filled, let the HPGe cool down over the course of at least 24 hours before turning on. Extra LN_2 will need to be added daily to keep the detector at operating temperatures.

4.2 Electronics

4.2.1 Desktop Module Power

In setting up the electronics system first the main desktop CAEN equipment was powered up and turned on. The three main pieces of equipment were the CAEN DT5423 desktop power distributer, CAEN DT5533E High Voltage (HV) power supply, and the CAEN DT5781 MCA. The power distributer and HV power supply were both powered through the Tripplite isolation transformer plugged directly into the wall outlet. The MCA was powered through a direct connection to a wall outlet. The DT5423 had no power switch and turned on immediately once powered, the other two devices had power switches on their backends. USB data acquisition cables were connected to the HV power supply and MCA to the computer for control.

4.2.2 Preamplifier and PMT Power

The preamplifiers and PMT's associated with the detectors were next powered on using the four low-voltage SubD9 connectors on the DT5423. Removal of the mounting hardware on the DB9 cables was sometimes necessary to make connections to the female connectors on the power distributer. It was important to make these connections now before biasing the detectors to avoid damaging the sensitive electronics.

4.2.3 Detector connections

The PIPSbox was connected to its associated preamplifier using two LEMO-00 to BNC connector, one for each detector. Bias voltage was provided to the preamplifier using two SHV cables that connected to the power supply. Data acquisition connections were made using two more LEMO-00 to BNC cables going from the energy out port on the preamplifier to the MCA.

The Canberra NaI(Tl) detectors required a SHV to BNC cable for data acquisition and a SHV cable for HV power. All connections were made directly into the PMT. The Scionix NaI(Tl) detectors did not require a DB9 connection as they not have a PMT that needs powering. They were connected using a BNC connector for the DAQ and a SHV cable for HV.

4.3 Software

Two programs were run for controlling the equipment used, the GECO2020 software for biasing detectors and the COMPASS software for configuring the data acquisition. Both programs were available to download for free from CAEN's website.

4.3.1 GECO2020

After launching the GECO2020 software the user must next connect the software to the HV board. Selecting the connect option under the File tab showed the box in the Figure 4.5.

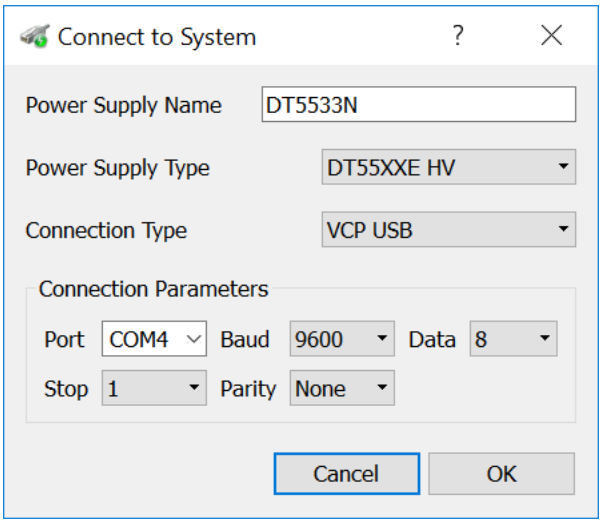

Figure 4.5 GECO2020 Board Connection

The power supply type was selected to be a DT55XXE model and connection type was set to be a USB connection. The port connection parameter depended on what port on the computer the USB cable was plugged into and was verified using the computer Device Manager. Baud rate and data were selected as 9600 and 8, respectively. After successful connection to the board the software displayed all available channels to be controlled as seen in Figure 4.6.

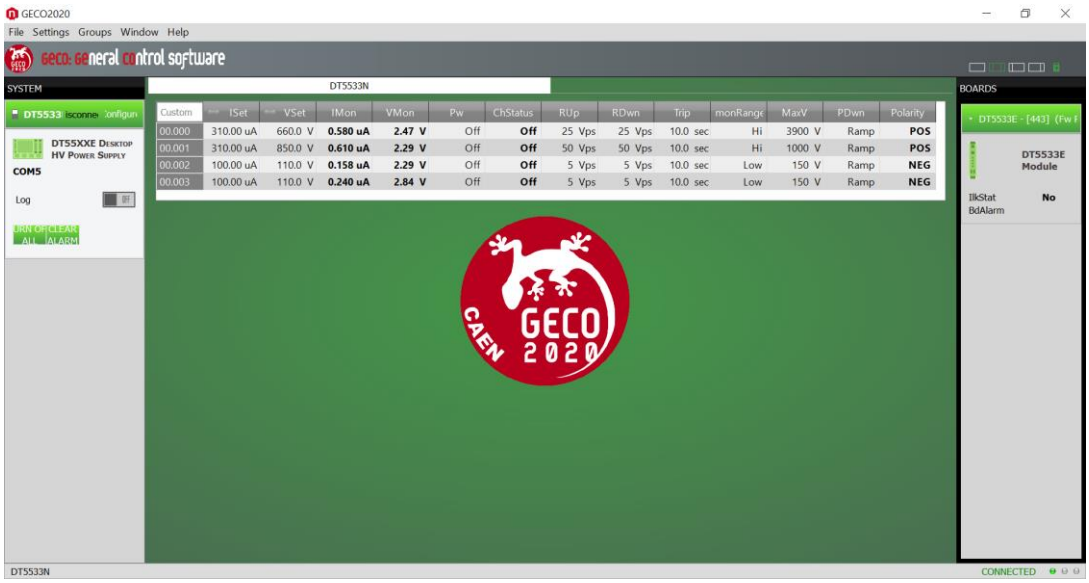

Figure 4.6 GECO2020 High Voltage Control Page

From this page the desired current and voltage could be set using ISet and VSet for each respective detector. A ramp up and ramp down voltage speed could be set as well as a maximum allowable voltage. When all settings were appropriately changed the bias voltage was applied to the detector using the power button. Polarity on this board model was not configurable, the first two channels could only bias positively and the last two could only bias negatively.

4.3.2 COMPASS

Launching and connecting the COMPASS software was done simply by pressing the connect all active boards button on the startup menu. After connecting the MCA, the user was taken to the acquisition page (Figure 4.7).

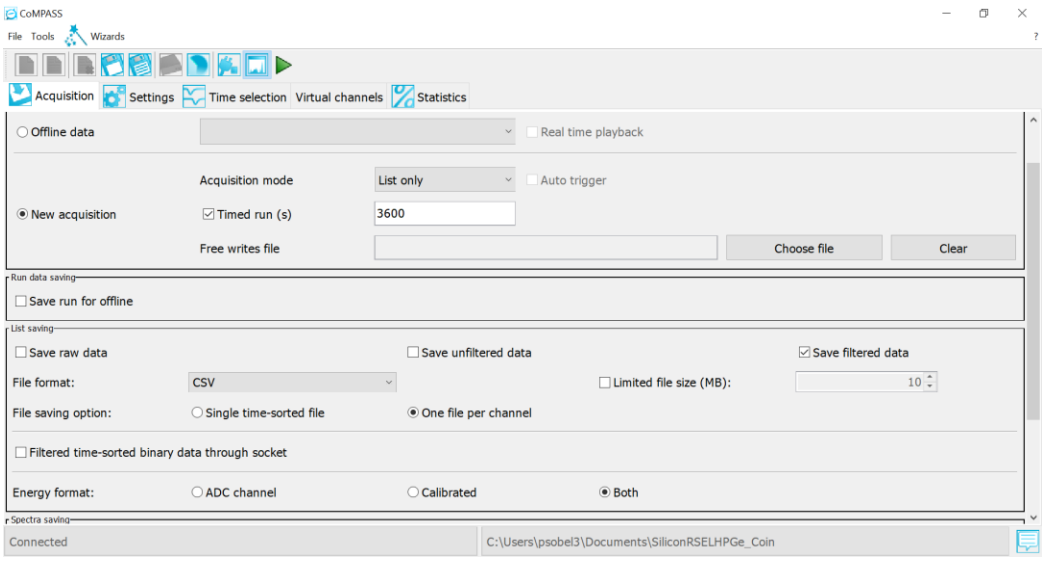

Figure 4.7 COMPASS Acquisition Page

The acquisition page allowed for selecting between two run modes, a wave mode, and a list mode. Wave mode allowed for seeing the incoming signal from the preamplifier and to track how modifying digital shaping parameters affected signal form. List mode was used for saving data collected during experiments in a variety of formats. Data was also able to be saved in raw, unfiltered, and filtered formats. An offline mode allowed for further data processing to be applied to a previously performed measurement. Digital signal shaping for each channel was performed in the Settings tab starting with the input.

Figure 4.8 Input Signal Parameters

The input signal tab (Figure 4.8) viewed on the waveform in waves mode could be modified using the record length and pre-trigger time periods which dictated what time was saved before and after each detected pulse. The number of baseline samples used to calculate the mean baseline of the signal was set here. The coarse gain set the amount of amplification applied to the input signal or the input dynamic range.

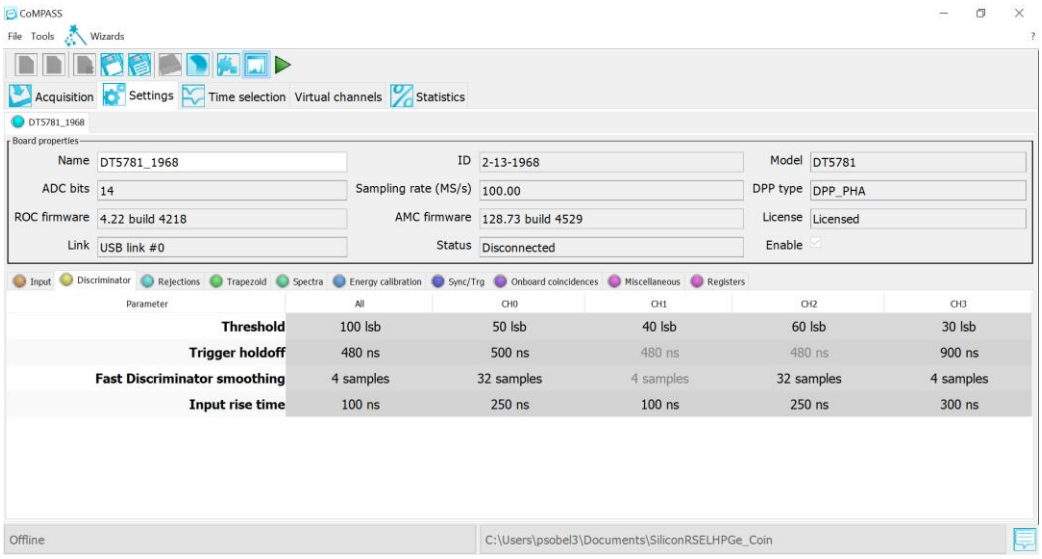

Figure 4.9 Discriminator Settings

The discriminator tab (Figure 4.9) controlled the settings for the RC-CR^2 timing signal shaping that decided whether an incoming pulse was counted or not. The threshold setting decided the least significant bit value which was defined by the noise level. Trigger holdoff values determined when a pulse could be accepted following the zero point of the previous pulse. The fast discriminator smoothing algorithm was used to determine the number of samples needed to create the RC-CR^2 signal, a tradeoff of signal amplitude to noise. The input rise time was set to match the timing signals rise time to the input signals rise time.

Figure 4.10 Rejection Settings

The rejections tab (Figure 4.10) worked with the built in CAEN software to forgo a received pulse based on the list of parameters provided. Saturation rejection canceled pulses received during the electronics deadtime and pileup rejections works to revoke pulses that have occurred close enough to stack their amplitudes. Energy high- and low-cut values allowed for discrimination based on the energy value, dictating a window of acceptable signals described by the user.

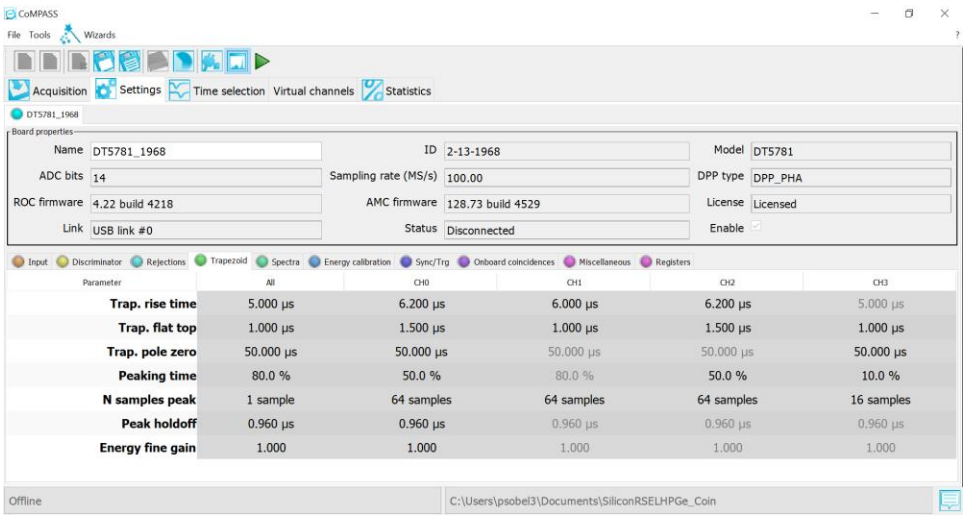

Figure 4.11 Trapezoidal Settings

The trapezoidal filtering parameters (Figure 4.11) described the shaped signal which would be used to identify the input energy of the preamplifier signal. All parameters here were applied in a Jordanov trapezoidal filter to convert the short rise-long tailed preamplifier signal into a trapezoid whose height from the baseline corresponded to the energy of the incident radiation. Settings used for beta-gamma coincidence in this case were optimized for high energy resolution and lower counting rates.

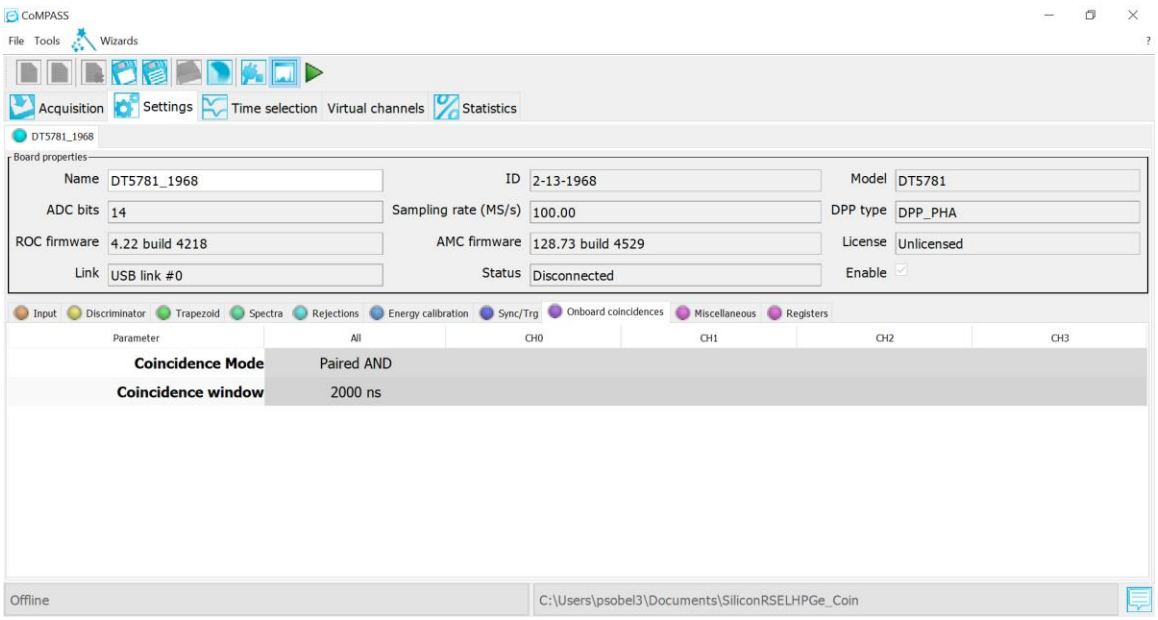

Figure 4.12 Onboard Coincidence settings

The CAEN DT5781 MCA allowed for coincidence to be performed on online data collected, only saving counts if they happened within the user defined coincidence timing window (Figure 4.12). The paired mode set the coincidence between pairs of channels and worked well for the silicon and photon detection systems. Coincidence window settings were optimized experimentally. The saved data was assigned the unfiltered category in the software.

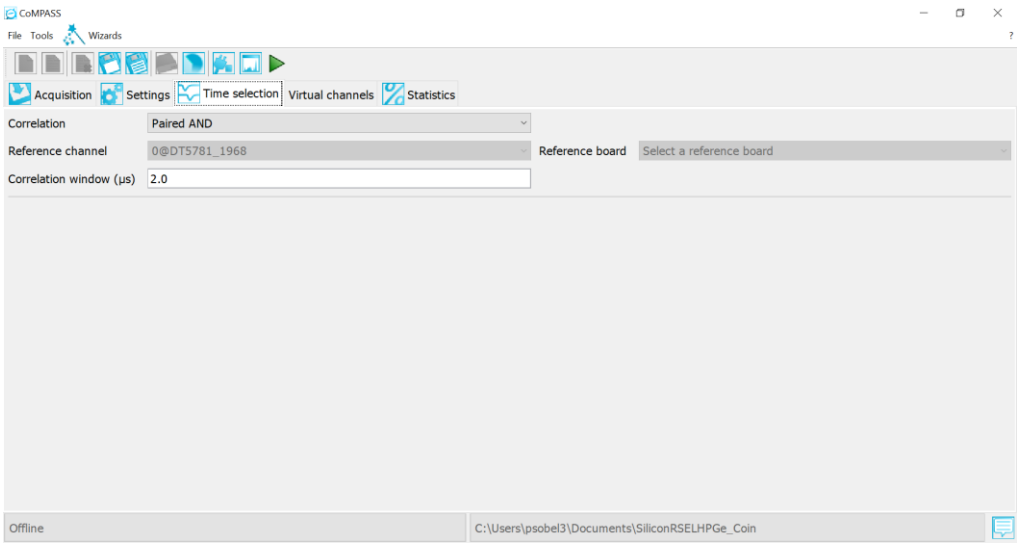

Figure 4.13 Time Selection Settings for 2D Spectra

The time selection tab (Figure 4.13) set the coincidence timing window parameters that were used to plot 2D spectra of the incoming radiation based on the channel pairs. This tab differed from the previous tab in that the 2D spectra collected here did not impact saved unfiltered data but only created a plot of the online data collected. Data saved from this mode was placed in the filtered data category.

Table 4.1 depicts the final parameters used in performing the measurements of ^{133}Xe. The parameters were settled on primarily using trial runs and comparing results over many measurements.

Table 4.1 COMPASS Parameters

Detector	PIPS #1	HPGe	PIPS #2	SCIONIX NaI(Tl)	Canberra NaI(Tl)
High Voltage	112.07	850.1	112.43	600	850.44
Input					
Record Length	50000	50000	50000	50000	50000
Pre-Trigger	1000	1000	1000	1000	1000
N Samples Baseline	4096	256	4096	256	256
DC Offset	20%	20%	20%	20%	20%
Coarse Gain	3x	10x	3x	33x	33x
Discriminator					
Threshold	50	40	60	30	100
Trigger Holdoff	500	480	480	900	300
Fast Discrim. Smoothing	32	4	32	4	32
Input Rise Time	250	100	250	300	500
Trapezoid					
Trap. Rise time	6.2	6	6.2	5	3
Trap. Flat Top	1.5	3	1.5	1	3
Trap. Pole Zero	30	50	30	50	50
Peaking Time	50%	80%	50%	10%	80%
N Samples Peak	64	64	64	16	16
Peak Holdoff	0.96	0.96	0.96	0.96	0.96
Energy Fine Gain	1	1	1	1	1
Spectra					
Energy N Channels	4096	4096	4096	1024	1024

4.4 Gas Manifold Operation

Control of the testing gas was done entirely mechanically; no valves or equipment utilized electrical switches. The main functions of the system as installed were the ability to evacuate the manifold and testing cell, purge the system with nitrogen for reducing memory effects, and injecting fresh radioxenon for performing measurements. Figure 4.14 depicts the different flow paths through the manifold for each function.

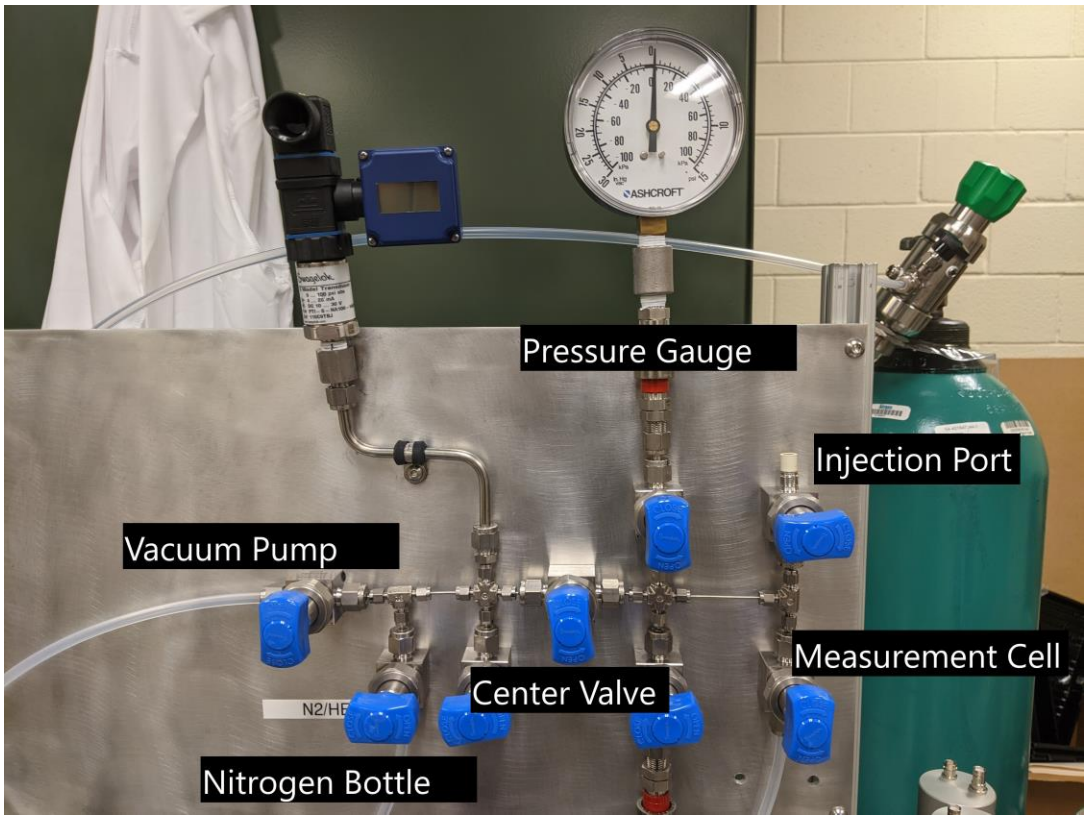

Figure 4.14 Gas Manifold Flow Paths

As a first step before injecting radioxenon the entire gas manifold needed to be put through a pump and flush procedure. The method used dry nitrogen gas to flush out the gas manifold lines, valves, and testing cell combined with multiple pumping cycles. The purpose of this procedure was to remove as much remaining radioactive gas sample and moisture from the system before doing an experimentation run. Once radioxenon was injected into the cell the system remained closed off from pumping until the measurement run was over.

The procedure for a pump and flush is given below, assuming all connections to the pump, the nitrogen regulator, and the testing cell had already been made.

1. Most valves should be closed from whatever previous test was performed, but if not, close all valves to avoid contaminating clean lines with radioactive gas.
2. Turn on the vacuum pump using the black switch at the base.
3. Once the pump has been on for a few minutes to allow it to reach full speed, open the first valve to begin pumping the clean gas side of the manifold. If the pressure regulator is attached the pressure being read out should begin to drop.
4. Open the valve to nitrogen fill line for a minute to evacuate any air that may be in the line. After a minute close that valve.
5. Open the central valve to begin pumping on the radioxenon side of the manifold, the valve to the pressure regulator should also be opened to get a read of the vacuum.
6. If the vacuum is stabilizing, meaning there are not any large leaks, the valve to the detection cell can be opened.
7. After a few minutes of pumping, open all other valves on the manifold that need to be cleaned out except for the nitrogen fill valve.
8. After another few minutes of pumping the entire system, the pressure in the system should sit at about -95 psi. Close the valve to the vacuum pump.
9. Open the nitrogen pressure regulator up until a very small flow of nitrogen gas is traveling into the system and let the manifold rise back up to just over atmospheric pressure. On the vacuum gauge this occurs when then needle travels just past the zero demarcation.
10. Close the nitrogen fill valve, the pressure regulator can be kept at the same position you had it. Let the system sit filled with nitrogen for about 2 minutes.

11. Open the vacuum valve again to the manifold and let it pump for about 5 minutes.
12. Repeat steps 8-11 at minimum five times to completely clean out the system. Once done close the vacuum valve for the last time.
13. The pump can be shut off and all valves can be closed.

After the flush and purge cycle had been performed enough times to clean out the system, radioxenon gas sample could be injected into the gas cell. The process of pulling some radioxenon sample out of the gas vial was done under the fume hood to capture any radioactive gas released when breaking the rubber septum. Equipment needed was a 100 µL gastight syringe and gloves. The procedure for injection of gas sample was as follows.

1. Turn the vacuum pump and give it a minute or two to reach top speed.
2. Open valves to the gas cell in order
    a. Vacuum pump valve
    b. Left manifold to right manifold valve
    c. Rubber septum injection valve
    d. Measurement cell valve
3. Allow the system to stabilize at its minimum pressure.
4. Close the valve between the left manifold and right side and finally close the vacuum valve.
5. With gloves on and working under the fume hood, puncture the rubber seal on the sample vial using the tip of the syringe in one straight motion to avoid leakage.
6. Pull a small amount of radioxenon from the center of the vial, on the order of 10-15 µL.

7. Retract the syringe from the sample vial without touching the plunger, walk the syringe over to the manifold.
8. Holding the syringe straight over the rubber septum injection port, push the needle slowly but firmly into the center of the of rubber bottom until the surface is broken.
9. Push the needle deeply into the injection port until it will not move further and then press the plunger down to inject radioxenon.
10. Once fully injected, retract the needle from the port. Hold the rubber septum down as the needle is pulled out to avoid losing unnecessary vacuum.
11. With the needle pulled out close the injection port valve.

With the gas injected the pressure gauge could be used to monitor the status of the measurement cell. Loss of vacuum did not become an issue for most trials until two weeks after closing the system.

CHAPTER 5. RESULTS

The contents of this chapter list the results of counting measurements performed using the two different detector setups. Measurements were performed on samples of ^{133}Xe and calibration of the detectors was done using calibration sources. Finally, an absolute efficiency calculation is performed to quantify the two detector setups.

5.1 Silicon-NaI(Tl) Beta-Gamma Coincidence

The Canberra NaI(Tl) detector was calibrated using ^{22}Na, and ^{137}Cs sources. Calibrating the PIPSbox was done in coincidence mode with the NaI(Tl) using a ^{137}Cs source. Peak beta energies along the ^{137}Cs beta-gamma spectrum represent the difference between the initial energy (661.7 keV) of the gamma and the energy deposited in the NaI(Tl) detector. Figure 5.1 depicts the beta-gamma spectrum produced for energy calibration.

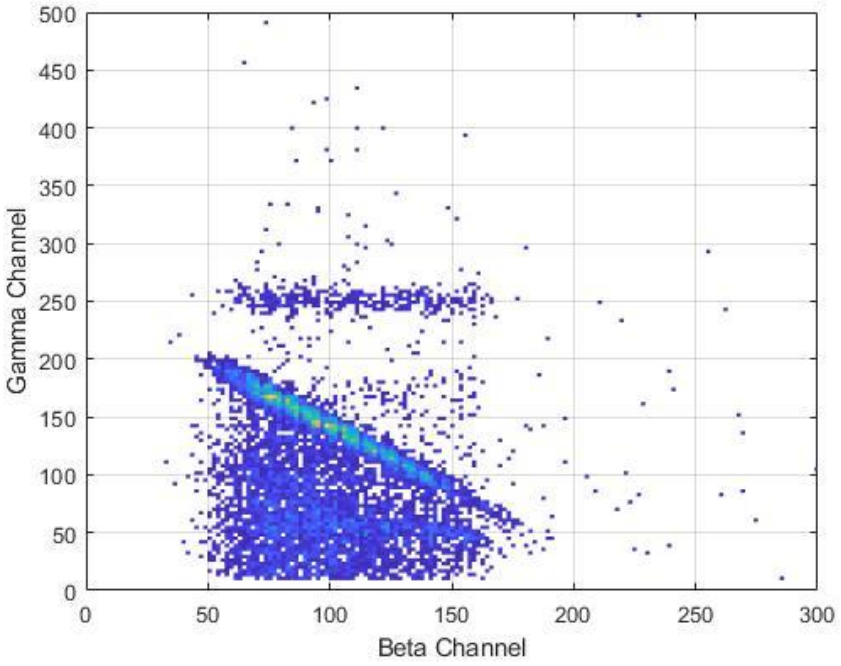

Figure 5.1 ^{137}Cs Beta-Gamma Coincidence Calibration Curve

Data saved from measurements of the ^{133}Xe sample were recorded in both a singles collection mode and a coincidence timing window mode simultaneously. Performing the absolute efficiency calculation requires knowledge of the isolated beta-singles and gamma-singles measurements in conjunction with the β-γ coincidence counts. The gamma-singles counts have three main features, the 30 keV X-ray peak, the 81 keV gamma-peak from ^{133}Xe, and the 163.2 keV gamma-peak from ^{131m}Xe. The X-ray peak of the gas measured using the NaI(Tl) cannot be split into ^{131m}Xe and ^{133}Xe X-rays due to the energy resolution of the detector. The 81 keV γ-peak is the second peak and is emitted in coincidence with the ^{133}Xe beta spectrum. The smallest peak at 163.9 keV is the single gamma-peak of ^{131m}Xe. This peak does not release in coincidence with an electron and thus mostly goes away in coincidence counting mode. Figure 5.2 show the measured gamma-singles with the NaI(Tl).

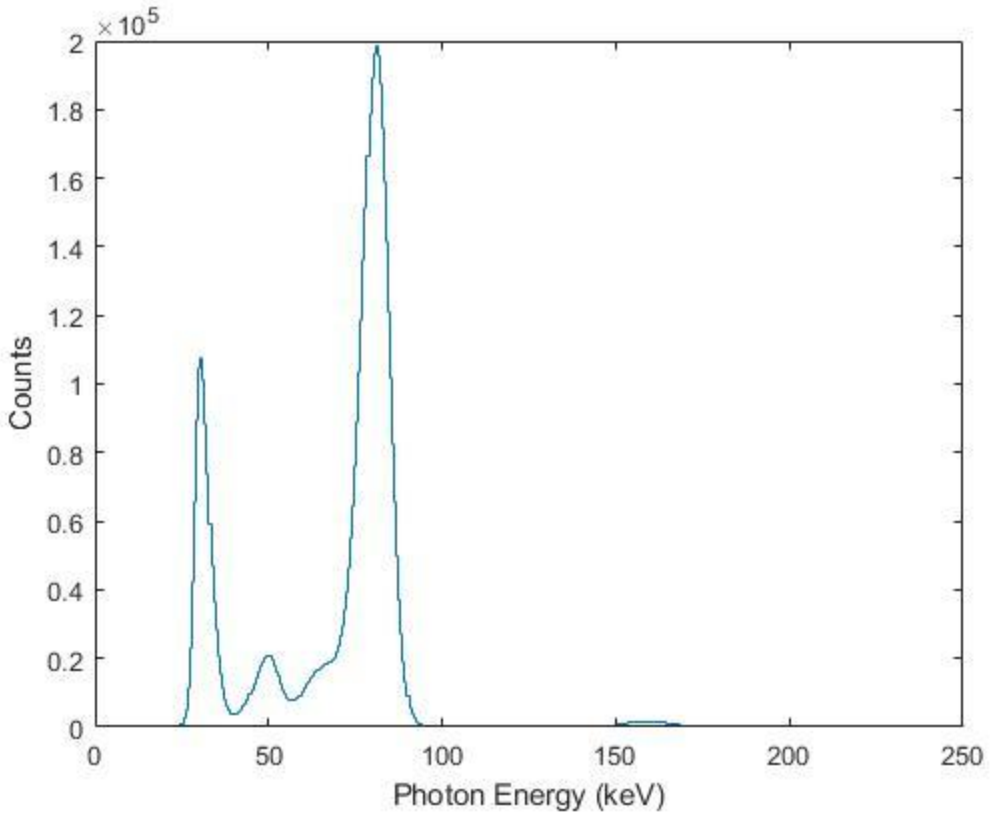

Figure 5.2 NaI(Tl) Gamma-Singles Spectrum (3 hour count)

The beta spectrum of the PIPSbox depicts two features, a small peak sitting on top of a large beta spectrum. The small peak represents the 129 keV conversion electrons from ^{131m}Xe, while the beta spectrum below it comes entirely from ^{133}Xe counts. Low energy beta counts are filtered out using the threshold settings in the COMPASS software. This was necessary to avoid high frequency noise that pervaded the silicon signal. Figure 5.3 depicts the beta-singles spectrum observed.

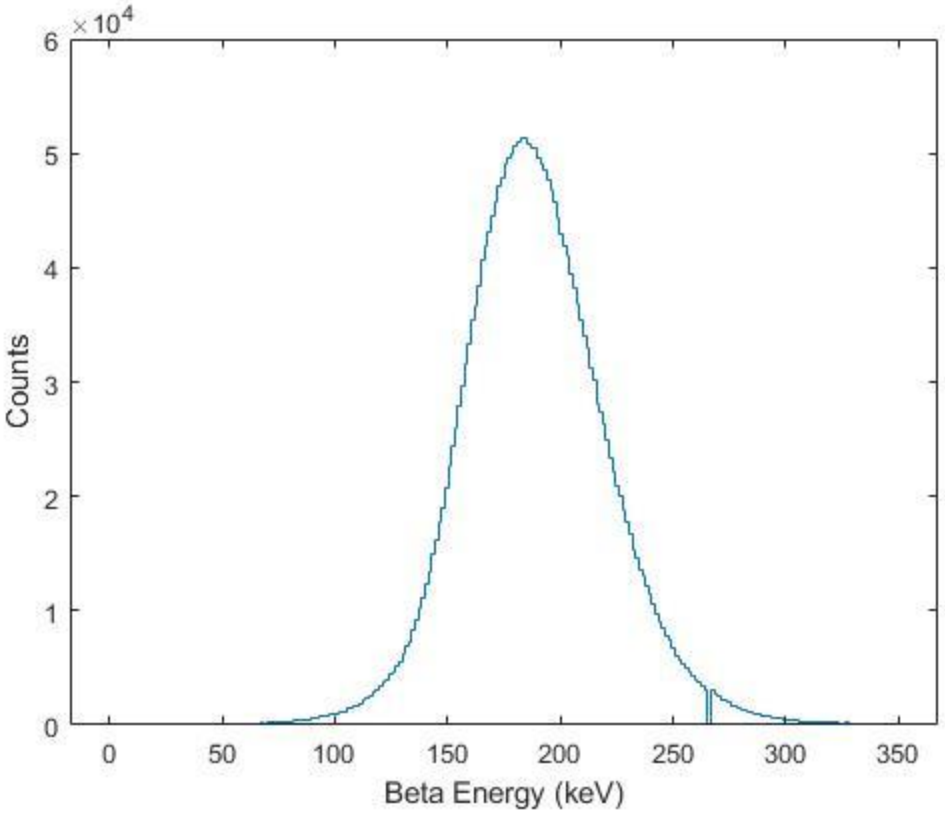

Figure 5.3 Silicon Beta-Singles Spectrum from ^{133}Xe (3 hour count)

The combined beta-gamma coincidence plot was measured using a 10 μs timing window. Displayed as a 2D spectrum of beta counts and gamma counts, the main features of Figure 5.4 are the ^{133}Xe coincidence region along the 81 keV γ-ray.

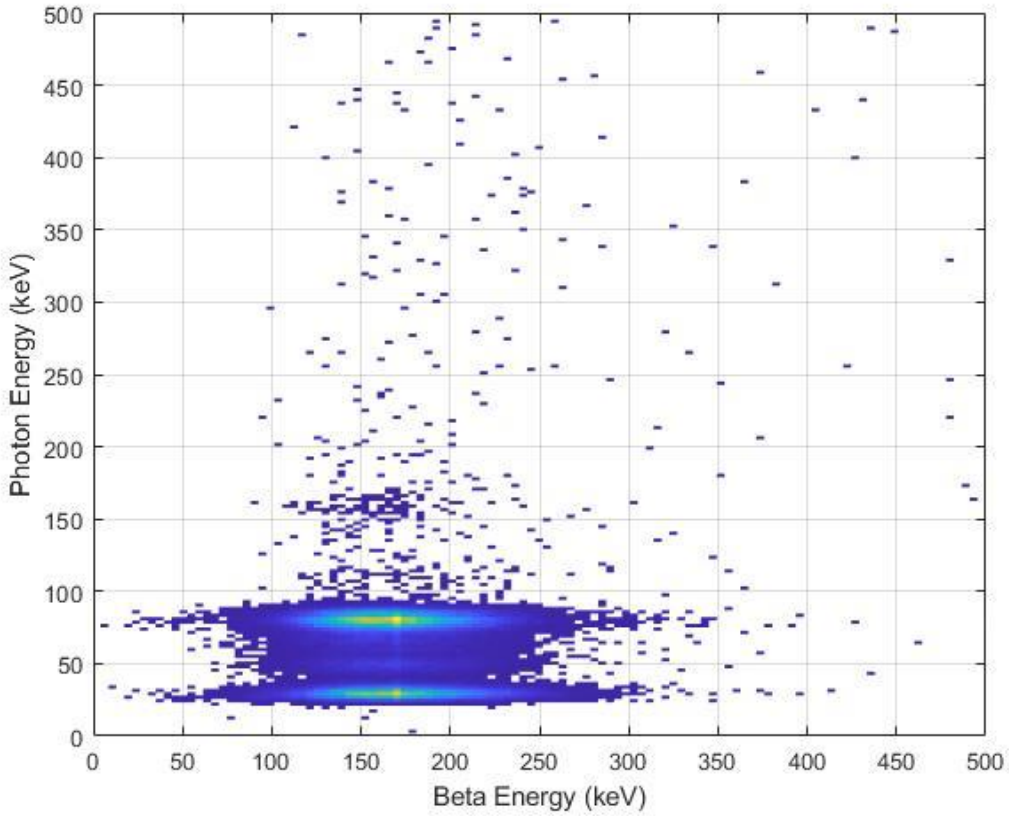

Figure 5.4 Beta-Gamma Spectrum (3 hour count)

5.2 Silicon-HPGe Beta-Gamma Coincidence

The HPGe was calibrated using ^{22}Na, ^{60}Co, and ^{137}Cs. Identified peaks were used to assign energy values to channel bins. Figure 5.5 depicts the gamma spectrum used. Each peak has a corresponding known energy value which is associated with the channel is appears in.

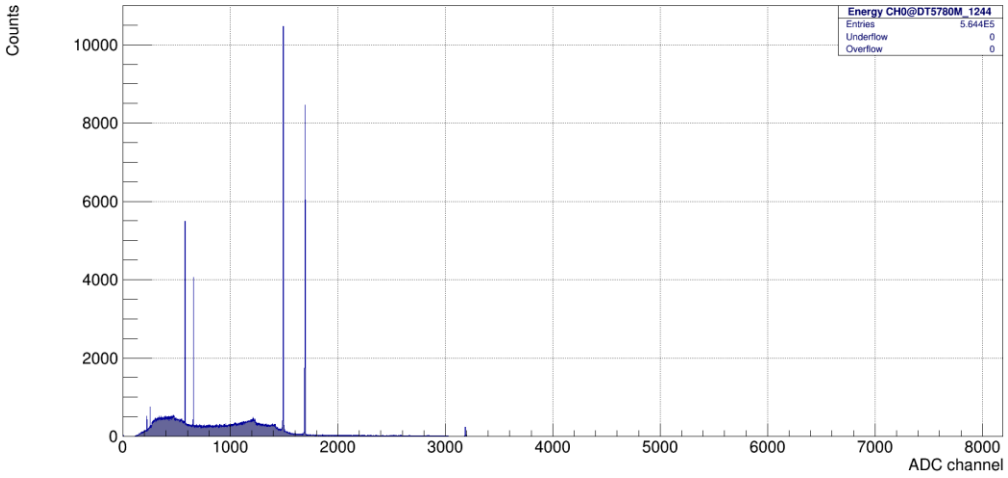

Figure 5.5 HPGe Calibration Gamma Spectrum

Using the now calibrated HPGe detector, the calibration for the PIPSbox was performed again. Similar to the NaI(Tl) setup, a ^{137}Cs source was measured in coincidence mode and the beta peaks were extracted from the 2D spectrum. Figure 5.6 depicts the beta-gamma spectrum obtained.

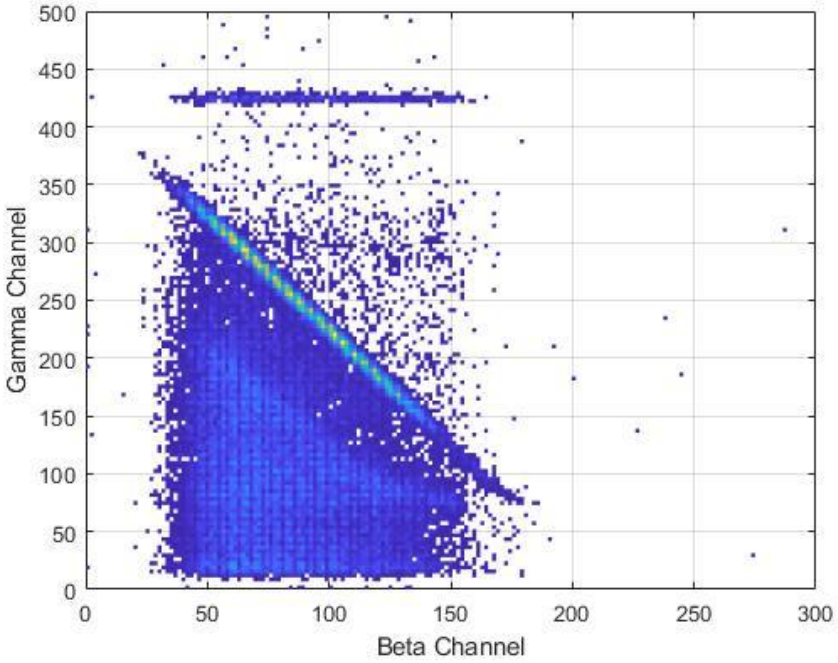

Figure 5.6 ^{137}Cs Beta-Gamma Calibration Spectrum

The HPGe singles xenon spectrum contained the same three main features as the NaI(Tl) spectrum. Energy resolution on all three peaks was much higher than the scintillator which was expected. The X-ray peaks on the HPGe spectrum were distinct, the ^{131m}Xe and ^{133}Xe x-rays were not merged as seen for the NaI(Tl). Figure 5.7 shows the γ-singles spectrum with the 81 keV gamma-ray, 163.2 gamma-ray, and two characteristic X-rays visible.

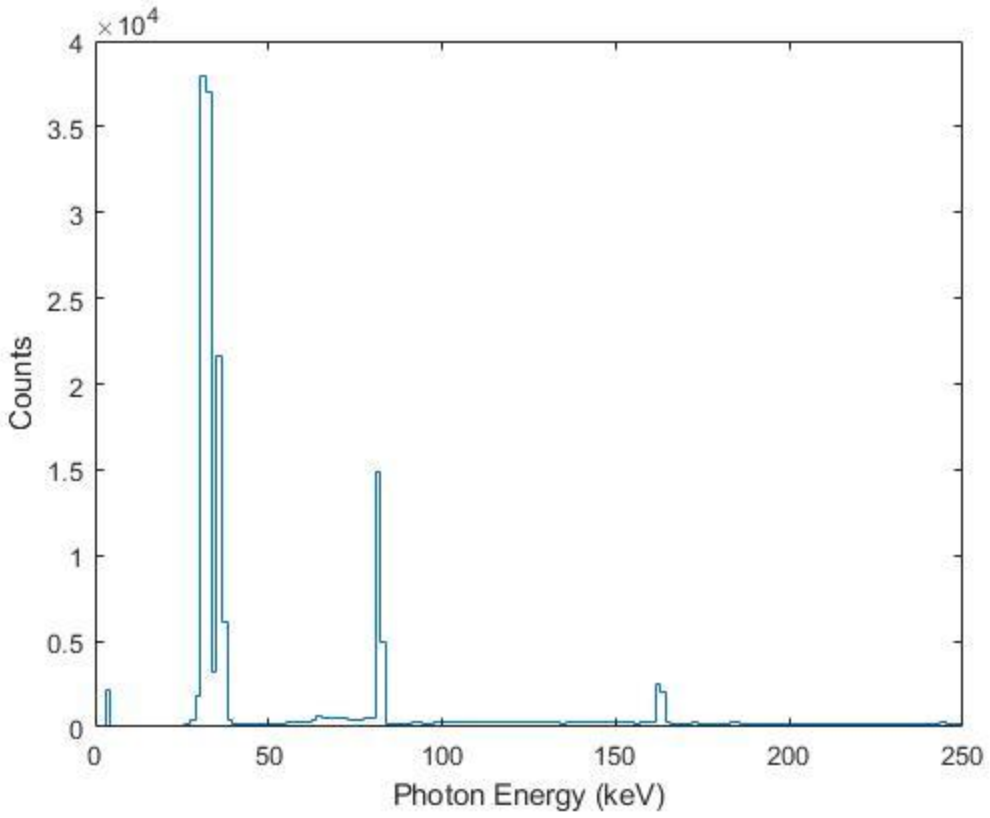

Figure 5.7 HPGe Gamma-Singles Counts (1 hour)

The beta spectrum as shown in Figure 5.8 produced by the PIPSbox during the HPGe coincidence measurements appears slightly different due to having occurred after many half-lives of ^{133}Xenon. The concentration of ^{131m}Xe in the sample vial increased to such an extent that the two conversion electrons of ^{131m}Xe, at 129 and 162 keV respectively, overshadowed the ^{133}Xe beta spectrum. A high threshold setting was used again, only allowing electrons of energies above around 80 keV to be detected. Height of the ^{131m}Xe 129 keV conversion electron peak should be taller than the 162 keV but is shrunk from being so close to the threshold energy set. Noise issues in the silicon were made worse when operating the detector in a flat orientation in comparison to the vertical orientation of the NaI(Tl) measurements.

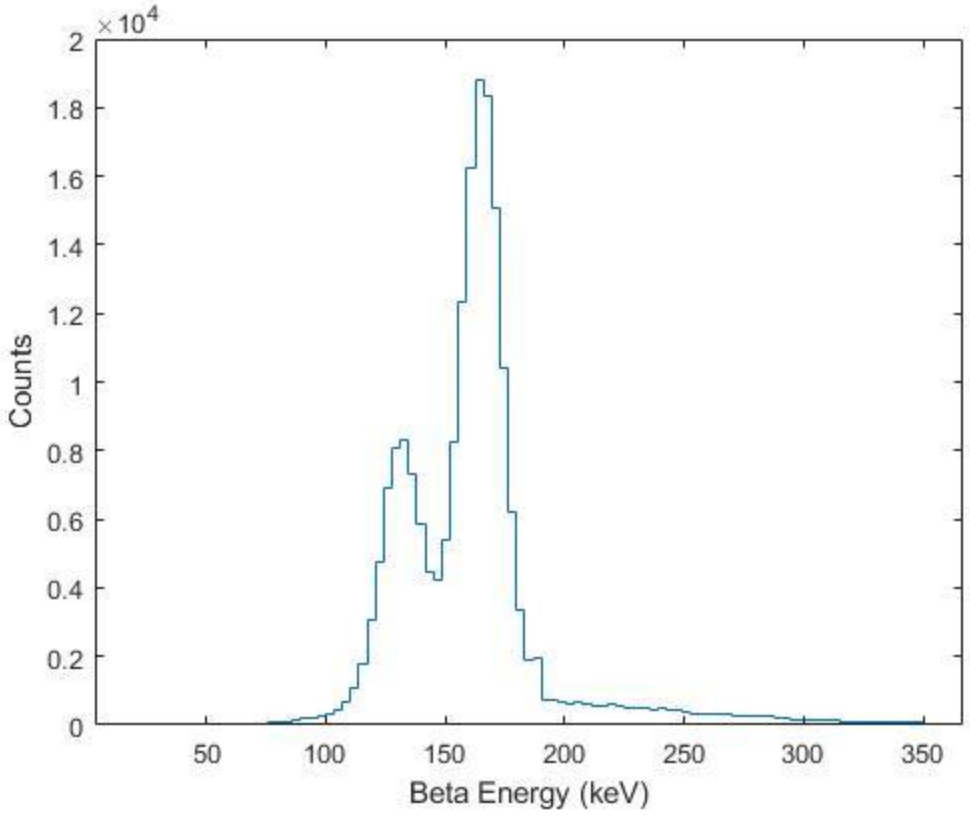

Figure 5.8 Silicon Beta-Singles Counts (1 hour)

Finally, a β-γ spectrum coincidence spectrum was produced using a 10 μs coincidence window. The ^{133}Xe region shrunk relative to the ^{131m}Xe region due to the amount decayed. The ^{131m}Xe 162 keV conversion electron vanished in coincidence mode due to it having no associated photon within the timing window. The ^{131m}Xe 129 keV CE appears as a tall peak over the X-ray spectrum. Lack of low energy electron counts means that most X-rays seen in coincidence will be produced from ^{131m}Xe, the 60 keV CE from ^{133}Xe was not detectable due to low energy noise issues requiring a high threshold. Figure 5.9 depicts the produced 2D beta-gamma spectrum.

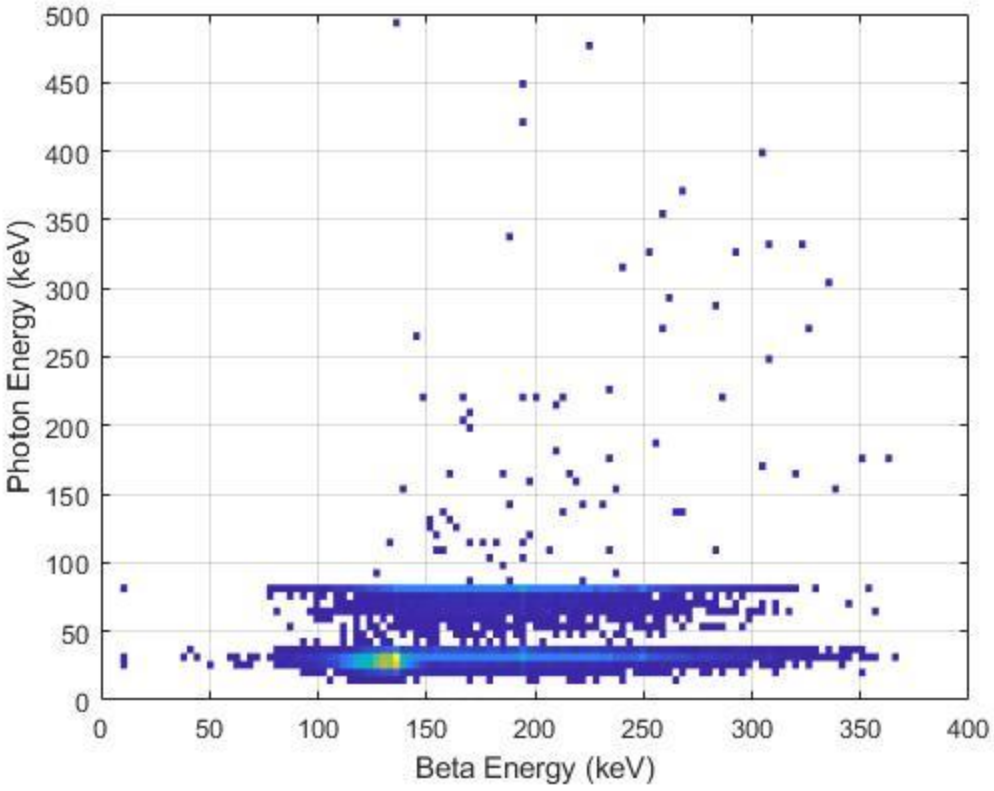

Figure 5.9 Silicon and HPGe Beta-Gamma Plot

5.3 Absolute Efficiency Calculation [17]

The absolute efficiency calculation provides performance metrics on how efficiently a beta-gamma coincidence setup measures each isotope of interest in a sample. The method used here to calculate the efficiency of the system relies on using actual radioxenon samples to make an absolute efficiency determination. The main source of uncertainty in performing these calculations for efficiency directly comes from uncertainties in the branching ratios of the different decay modes. For this work the absolute efficiency of

detecting ^{133}Xe was calculated from the coincidence spectrum produced by its 81 keV gamma-ray.

The absolute efficiency for detection of the 81 keV gamma-ray is calculated using efficiencies of detecting the beta particles and gamma-rays separately. Equation 5.1 describes this relationship where $\varepsilon_{\beta\gamma 81}$ is the absolute 81 keV beta-gamma efficiency, ε_{β} is the beta efficiency and $\varepsilon_{\gamma 81}$ is the gamma efficiency.

$$\varepsilon_{\beta\gamma 81} = \varepsilon_{\beta} * \varepsilon_{\gamma 81} \qquad \textbf{Equation 5.1}$$

The beta efficiency describes ratio of beta particles accepted in the coincidence measurement to total singles seen. The calculation for the beta efficiency is given in equation 5.2, with $C_{\beta\gamma 81}$ being the total counts in the 81 keV beta-gamma peak and $C_{\gamma 81}$ representing the total counts in the gamma-singles peak.

$$\varepsilon_{\beta} = \frac{C_{\beta\gamma 81}}{C_{\gamma 81}} \qquad \textbf{Equation 5.2}$$

Calculating the 81 keV gamma-ray efficiency takes some more math, as finding the ratio of the beta particles accepted means factoring in the branching ratios of the other decay modes. The used branching ratio values for the calculation are provided in table 5.1.

Table 5.1 Branching Ratio Values [17]

Decay Modes	Branching Ratio
Gamma-81	0.38 ± 0.007
Gamma-32	0.4876 ± 0.0145
Beta	0.999 ± 0.014
CE-76	0.100936 ± 0.002068
Auger-25	0.052 ± 0.004

Simplification of the gamma-ray efficiency calculation is made by assuming 100% efficiency of the conversion electrons and auger electrons. The calculation for the efficiency is given in equation 5.3.

$$\varepsilon_{\gamma 81} = \frac{C_{\beta\gamma 81} * \left(1-\left(1-BR_{\beta} * \varepsilon_{\beta}\right) * \left(-BR_{CE76}-BR_{\gamma 32}+\left(1-BR_{Auger25}\right)^{2}\right)\right)}{BR_{\gamma 81} * \varepsilon_{\beta} * C_{\beta}} \qquad \textbf{Equation 5.3}$$

Data used to perform the calculations contained beta-gamma coincidence measurements of both PIPS detectors in coincidence with either one NaI(Tl) detector or one HPGe detector. Background was removed from the gamma-singles counts using a fit line to the surrounding background counts in the spectrum. Superimposed conversion electron peaks on the beta spectrum were removed using line fits to the beta spectrum counts. Beta efficiency was calculated from the measurements performed with the HPGe detector and applied to both as the setups are theoretically similar. The results of the efficiency calculations are provided in table 5.2.

Table 5.2 Absolute Efficiency Results

Detectors	Beta Efficiency	Gamma Efficiency	B-γ Efficiency	Uncertainty (%)
x2 Silicon – NaI(Tl)	0.10197	0.31164	0.031777931	0.3042
x2 Silicon-HPGe	0.10197	0.4505	0.045937	0.0762

Efficiency of detecting the 81 keV gamma-ray according to Cooper was 0.81959 for an almost 4π detection geometry. McIntyre using a slightly different efficiency calculation method applied to the ARSA system found a beta efficiency of 0.927 and a gamma efficiency of 0.597 [18].

Low beta efficiency of the systems could be the result of large energy rejection thresholds set to keep the accepted signals above the silicon noise. Photon counts significantly dwarfed beta counts in most measurements giving poor β-γ efficiency statistics. Photon detection efficiency was more in line with expected results, especially given the larger surface area of the HPGE (38 cm^2) to the NaI(Tl) (20.26 cm^2).

CHAPTER 6. CONCLUSIONS

Included here is a summary of completed work and the conclusions drawn. A section for potential future work is included as well.

6.1 Conclusions

A complete, viable radioxenon forensics lab has been created at Georgia Tech which was utilized to perform spectroscopy of two xenon isotopes. Procedures were developed to measure samples of radioactive gas in a controlled environment using both NaI(Tl) detectors as well as an HPGe. The PIPSbox was characterized over numerous measurements of radioxenon gas and calibration sources to find optimum settings for high resolution measurements. Grounding and shielding techniques were utilized to minimize the noise characteristics of silicon. Results show that noise reduction in silicon is of upmost importance for measuring low energy electrons.

Spectra produced by the detection setups showed that unique signatures of ^{131m}Xe and ^{133}Xe could be distinguished using beta-gamma spectroscopy with a 10 μs coincidence window. With the HPGe detector, the separate x-rays of ^{133}Xe and ^{131m}Xe were observable. The silicon detector could distinguish the 129 and 163 keV conversion electron peaks from ^{131m}Xe on top of the beta spectrum. Absolute beta-gamma efficiencies were calculated as 3.17% and 4.59% for the NaI(Tl) and HPGe detection setups, respectively.

6.2 Future Work

Noise reduction in the silicon detectors would be the first place to start in bringing this laboratory in a position to produce more refined results. At such a high energy threshold for counts particles such as the ^{133}Xe 45 keV conversion electron are lost, removing some of the ability to perform analysis of the spectra. Testing could include the addition of another high-resolution spectroscopy preamplifier to compare against the Mirion one. A beta-gamma simulation using codes such as MCNP-POLIMI to estimate the best-case absolute efficiency could be also performed.

With a reduction in noise threshold the ^{133}Xe X-ray efficiency could be calculated, as well as the absolute efficiency for the decays of ^{131m}Xe. Bringing in gas samples of all four radioxenon isotopes to be detected would then allow for full efficiency calculations. Measurements of the minimum detectable activity of each isotope could be compared against other major beta-gamma systems.

APPENDIX A. MATLAB SCRIPT

```
% Beta-Gamma Offline Coincidence

tau = 5e+6; % time difference between radiation (ps)

bt = length(betatime1); % number of elements
gt = length(gammatime);

agpeak = histcounts(gammaenergy,4096);
gammapeaktotal = sum(agpeak(50:62));
gs = 1;

for jj = 1: bt
    countcheck(jj) = jj;

        for ii = gs : gt
         dtt = abs(betatime1(jj)-gammatime(ii)); % time difference
between peaks
         if dtt <= tau

            betacoin1(jj) = betaenergy1(jj);
            gammacoin1(jj) = gammaenergy(ii);
            break
            gs = ii+1;
         end

        end
end
truebetacoin1 = nonzeros(betacoin1);
truegammacoin1 = nonzeros(gammacoin1);
tgc1 = histcounts(truegammacoin1,4096);
gammapeak1 = sum(tgc1(50:62));

bt1 = length(betatime2); % number of elements
gt1 = length(gammatime);


for jj = 1: bt1
    countcheck(jj) = jj;

        for ii = 1 : gt1
         dtt = abs(betatime2(jj)-gammatime(ii)); % time difference
between peaks
         if dtt <= tau

            betacoin2(jj) = betaenergy2(jj);
            gammacoin2(jj) = gammaenergy(ii);

            break
         end
```

```
        end
end
truebetacoin2 = nonzeros(betacoin2);
truegammacoin2 = nonzeros(gammacoin2);
tgc2 = histcounts(truegammacoin2,4096);
gammapeak2 = sum(tgc2(50:62));
gammapeakcoin = gammapeak1+gammapeak2;
betaefficiency = gammapeakcoin/gammapeaktotal
```

REFERENCES

[1] Saey, P.R.J, and De Geer, L.-E. "Notes on Radioxenon Measurements for CTBT Verification Purposes." Applied Radiation and Isotopes 63.5 (2005): 765-73. Web.

[2] Saey, P.R. (2011). Xenon: Radionuclides. In Encyclopedia of Inorganic and Bioinorganic Chemistry, R.A. Scott (Ed.). https://doi.org/10.1002/9781119951438.eibc0427

[3] Bowyer, T. W. "A Review of Global Radioxenon Background Research and Issues." Pure and Applied Geophysics (2020): Pure and Applied Geophysics, 2020-02-24. Web.

[4] Kalinowski, M. B. and M. P. Tuma (2009). "Global radioxenon emission inventory based on nuclear power reactor reports." J Environ Radioact 100(1): 58-70.

[5] Biegalski, S.R., et al., Analysis of data from sensitive U.S. monitoring stations for the Fukushima Daiichi nuclear reactor accident, Journal of Environmental Radioactivity (2011), doi:10.1016/j.jenvrad.2011.11.007

[6] Saey, P. R. (2009). "The influence of radiopharmaceutical isotope production on the global radioxenon background." J Environ Radioact 100(5): 396-406.

[7] Biegalski, S. R. F., et al. (2012). "Tracers for radiopharmaceutical production facilities." Journal of Radioanalytical and Nuclear Chemistry 296(1): 477-482.

[8] Ringbom, A, Elmgren, Klas, Lindh, Karin, Peterson, Jenny, Bowyer, Theodore W, Hayes, James C, McIntyre, Justin I, Panisko, Mark, and Williams, Richard. "Measurements of Radioxenon in Ground Level Air in South Korea following the Claimed Nuclear Test in North Korea on October 9, 2006." Journal of Radioanalytical and Nuclear Chemistry 282.3 (2009): 773-79. Web.

[9] Auer, Matthias, Kumberg, Timo, Sartorius, Hartmut, Wernsperger, Bernd, and Schlosser, Clemens. "Ten Years of Development of Equipment for Measurement of Atmospheric Radioactive Xenon for the Verification of the CTBT." Pure and Applied Geophysics 167.4-5 (2010): 471-86. Web.

[10] Cooper, Matthew W, McIntyre, Justin I, Bowyer, Ted W, Carman, April J, Hayes, James C, Heimbigner, Tom R, Hubbard, Charles W, Lidey, Lance, Litke, Kevin E, Morris, Scott J, Ripplinger, Michael D, Suarez, Reynold, and Thompson, Robert. "Redesigned β–γ Radioxenon Detector." Nuclear Instruments & Methods in Physics Research. Section A, Accelerators, Spectrometers, Detectors and Associated Equipment 579.1 (2007): 426-30. Web.

[11] McIntyre, J I, Abel, K H, Bowyer, T W, Hayes, J C, Heimbigner, T R, Panisko, M E, Reeder, P L, and Thompson, R C. "Measurements of Ambient Radioxenon Levels Using the Automated Radioxenon Sampler/analyzer (ARSA)." Journal of Radioanalytical and Nuclear Chemistry 248.3 (2001): 629-35. Web.

[12] Popov, Yu, Kazarinov, N, Popov, V, Rykov, Yu, and Skirda, N. "Measuring Low Activities of Fission-Product Xenon Isotopes Using the Beta-gamma Coincidence Method." Instruments and Experimental Techniques 48.3 (2005): 380-86. Web.

[13] Ringbom, A, Larson, T, Axelsson, A, Elmgren, K, and Johansson, C. "SAUNA—a System for Automatic Sampling, Processing, and Analysis of Radioactive Xenon." Nuclear Instruments & Methods in Physics Research. Section A, Accelerators, Spectrometers, Detectors and Associated Equipment 508.3 (2003): 542-53. Web.

[14] Bläckberg, L., et al. (2011). "Investigations of surface coatings to reduce memory effect in plastic scintillator detectors used for radioxenon detection." Nuclear Instruments and Methods in Physics Research Section A: Accelerators, Spectrometers, Detectors and Associated Equipment 656(1): 84-91.

[15] Fontaine, J.-P, Pointurier, F, Blanchard, X, and Taffary, T. "Atmospheric Xenon Radioactive Isotope Monitoring." Journal of Environmental Radioactivity 72.1 (2004): 129-35. Web.

[16] Cagniant, A, Le Petit, G, Gross, P, Douysset, G, Richard-Bressand, H, and Fontaine, J.-P. "Improvements of Low-level Radioxenon Detection Sensitivity by a State-of-the Art Coincidence Setup." Applied Radiation and Isotopes 87 (2014): 48-52. Web.

[17] Cooper, M. W, Ely, J. H, Haas, D. A, Hayes, J. C, McIntyre, J. I, Lidey, L. S, and Schrom, B. T. "Absolute Efficiency Calibration of a Beta-Gamma Detector." IEEE Transactions on Nuclear Science 60.2 (2013): 676-80. Web.

[18] McIntyre, Justin I, Cooper, Mathew, Carman, April J, Bowyer, Theodore W, Day, Anthony, Haas, Derek, Hayes, James C, Heimbigner, Tom R, Hubbard, Charlie, Litke, Kevin, Ripplinger, Michael, Schrom, Brian, and Suarez, Reynold. "Concentration Independent Calibration of β–γ Coincidence Detector Using 131mXe and 133Xe." Journal of Radioanalytical and Nuclear Chemistry 282.3 (2009): 755-59. Web.